Review

Not peer-reviewed version

$Ti_3C_2T_x$ MXene-Based Hybrid Photocatalysts in Organic Dye Degradation: A Review

Tank Seling , Mackenzie Songsart-Power , Amit Shringi , Janak Paudyal , Fei Yan * , Tej B. Limbu *

Posted Date: 18 February 2025

doi: 10.20944/preprints202502.1240.v1

Keywords: Ti3C2Tx MXene; Dye Degradation; Photocatalysis; Charge Separation

 doi:10.20944/preprints202502.1240.v1

Review

$Ti_3C_2T_x$ MXene-Based Hybrid Photocatalysts in Organic Dye Degradation: A Review

Tank Seling [1], Mackenzie Songsart-Power [2], Amit Shringi [1], Janak Paudyal [3], Fei Yan [1,*] and Tej B. Limbu [2,*]

[1] Department of Chemistry and Biochemistry, North Carolina Central University, NC 27707, United States
[2] Department of Physical and Applied Sciences, University of Houston-Clear Lake, TX 77058, United States
[3] Department of Chemistry and Physics, McNeese State University, Lake Charles, LA 70605, United States
* Correspondence: fyan@nccu.edu (F.Y.); tejblimbu@gmail.com (T.B.L.)

Abstract: This review provides an overview of the fabrication methods for $Ti_3C_2T_x$ MXene-based hybrid photocatalysts and evaluates their role in degrading organic dye pollutants. $Ti_3C_2T_x$ MXene has emerged as a promising material for hybrid photocatalysts due to its high metallic conductivity, excellent hydrophilicity, strong molecular adsorption, and efficient charge transfer. These properties facilitate faster charge separation and minimize electron-hole recombination, leading to exceptional photodegradation performance, long-term stability, and significant attention in dye degradation applications. $Ti_3C_2T_x$ MXene-based hybrid photocatalysts significantly improve dye degradation efficiency, as evidenced by higher percentage degradation and reduced degradation time compared to conventional semiconducting materials. This review also highlights computational techniques employed to assess and enhance the performance of $Ti_3C_2T_x$ MXene-based hybrid photocatalysts for dye degradation. It identifies the challenges associated with $Ti_3C_2T_x$ MXene-based hybrid photocatalyst research and proposes potential solutions, outlining future research directions to address these obstacles effectively.

Keywords: $Ti_3C_2T_x$ MXene; dye degradation; photocatalysis; charge separation

1. Introduction

The fast-growing industrialization has increased the generation of highly toxic and carcinogenic wastewater[1]. Discharging untreated wastewater from textile, pharmaceutical, dying, and paper printing industries leads to increased dyes in the water sources, causing a severe threat to the environment[2]. It contains chromophores for color and auxochromes for fiber affinity, harming aquatic life by coloring water, blocking sunlight, and disrupting photosynthesis, which is crucial for ecosystems [3]. Discharged dyes are categorized into cationic dyes (e.g., methylene blue (MB), crystal violet (CV), rhodamine B (RhB)) that carry positive charges, are widely used in textiles, and pose toxicity risks. Anionic dyes (e.g., acid orange 7 (AO7), acid blue 92 (AB92), Congo red (CR)) carry negative charges, exhibit water solubility, and are challenging to remove [4]. To get rid of these dyes, various degradation approaches like membrane filtration, oxidation, adsorption, and photocatalysis have been successfully developed and demonstrated [5,6].

Photocatalysis is one of the best degradation methods because it is eco-friendly and cost-effective for degrading organic pollutants [7]. Numerous studies have focused on developing photocatalytic materials with a wide energy bandgap, abundant surface active sites, and efficient charge separation capabilities to optimize the photodegradation of dyes. [8]. Single-component semiconducting photocatalysts such as TiO_2, ZnO, ZnS, SnO_2, g-C_3N_4, and CdS have been extensively used[9,10]. However, the photocatalytic activity of these single semiconducting materials is generally limited by poor visible light absorption and utilization, as well as rapid charge recombination and low electron-hole mobility [11,12]. To improve the photocatalytic performance of these single semiconducting

 doi:10.20944/preprints202502.1240.v1

materials, various strategies such as the construction of heterojunction[13], doping of elements[14], and introduction of co-catalyst[14] have been proposed and explored.

The photocatalytic activity of semiconducting materials can be effectively enhanced by modifying them with a co-catalyst[15]. The presence of a co-catalyst prevents the recombination between electrons and holes, which is otherwise inevitable by facilitating the separation of the charge. Various materials such as graphene[16], carbon nanotubes[17], and carbon quantum dots[18], have been used as co-catalysts to enhance the efficiency of the photocatalytic degradation of dyes. Although significant advancements have been made with the above-mentioned co-catalysts, they are somehow limited due to the scarcity of functional groups and sufficient conductivity[19]. The lack of sufficient surface functional group restricts the strong chemical bond between photocatalyst and co-catalyst and the lower electrical conductivity impedes charge migration within the material. Both factors play a crucial role in reducing photocatalytic efficiency. Therefore, there is still a need for efficient and inexpensive co-catalysts to increase the photocatalytic efficiency of degradation of the organic dyes.

MXenes, especially $Ti_3C_2T_x$, have been considered excellent component material for the fabrication of the hybrid photocatalyst due to their lower fermi level than most studied semiconductors, the presence of abundant terminal functional groups, excellent metallic conductivity and exposed terminal metal sites[20–22]. MXenes are a class of two-dimensional (2D) layered materials consisting of transition metal carbides, nitrides, or carbonitrides, which are represented by a general formula, $M_{n+1}X_n$ (n = 1, 2, 3), where M represents a transition metal (such as Sc, Ti, Zr, Hf, V, Nb, Ta, or Mo), and X corresponds to carbon, nitrogen, or carbonitride. The presence of abundance functional groups such as −OH, −O, and −F on $Ti_3C_2T_x$ MXene facilitates the strong interfacial chemical bonding with semiconductors which enables the formation of a Schottky junction that acts as an electron trap, thereby suppressing the recombination of photoexcited electron-hole pairs[23]. The excellent metallic conductivity of $Ti_3C_2T_x$ MXene ensures rapid charge carrier migration, promoting efficient separation of photogenerated electrons and holes[24]. Moreover, exposed terminal metal sites enhance reactivity compared to carbon-based materials, making $Ti_3C_2T_x$ MXene a more effective co-catalyst.

$Ti_3C_2T_x$ MXene has limited effectiveness as a standalone photocatalyst, as it requires doping and UV radiation to function optimally [25]. However, when incorporated into composite photocatalysts, its role extends beyond serving as a mere photogenerated charge acceptor co-catalyst. Due to its large surface area and surface functionalities, $Ti_3C_2T_x$ MXene provides the superior growing platform for uniform, size-controlled, and fine dispersion of photocatalysts which exposes more surface-active sites of composite photocatalyst [26–29]. Additionally, $Ti_3C_2T_x$ MXene possesses distinctive physical and chemical properties, including high electrical conductivity, excellent hydrophilicity, mechanical stability, ion intercalation ability, and tunable surface functionalization [30–32]. These attributes make it an ideal candidate for use in composite photocatalyst materials. The integration of $Ti_3C_2T_x$ MXene with semiconducting materials has resulted in hybrid photocatalysts featuring micro/nano architectures and multi-junction nanocomposites. These hybrid photocatalyst materials leverage synergistic interactions of $Ti_3C_2T_x$ MXene with conventional semiconductors, or metal nanostructures, enabling enhanced charge separation and reduced recombination rates [21,33]. These characteristics make $Ti_3C_2T_x$ MXene-based hybrid photocatalysts highly effective for the photodegradation of cationic and anionic organic pollutants [34].

This review explores $Ti_3C_2T_x$ MXene-based hybrid photocatalysts for the degradation of cationic and anionic organic dyes. It covers the synthesis of $Ti_3C_2T_x$ MXene, its integration into hybrid photocatalysts, its role and effectiveness in dye degradation, and the associated mechanisms. Additionally, it discusses the challenges and opportunities in this area while providing insights into potential future research directions.

 doi:10.20944/preprints202502.1240.v1

2. $Ti_3C_2T_x$ MXene and Synthesis Methods

2.1. Introduction to $Ti_3C_2T_x$ MXenes

MXenes, first synthesized by Naguib et al. in 2011, are two-dimensional crystals of transition metal carbides, nitrides, or carbonitrides[35]. These novel 2D materials are synthesized by top-down approaches beginning with their three-dimensional parent material known as MAX. MAX phases are transition metal carbides, nitrides, or carbonitrides with the general formula $M_{(n+1)}AX_n$, n = 1, 2, or 3, where M denotes an early transitional metal such as titanium (Ti), niobium (Nb), molybdenum (Mo), tantalum (Ta), vanadium (V), or chromium (Cr), A refers to an A group element (mainly 13 and 14 group), and X represents a carbon, nitrogen, or carbonitride that intersperses the M layers[36]. When the A layers are removed from the MAX phase through chemical etching, 2D crystals are formed. However, most of the synthesis methods involve an aqueous medium, resulting in the surface termination of the M elements on the obtained 2D MXene crystals. These MXene crystals are represented by the general formula, $M_{(n+1)}X_nT_x$, n = 1, 2, or 3, where T_x refers to surface terminations, mostly -OH, -O, and -F [37–41].

MXenes have gained considerable attention for their exceptional properties, such as hydrophilicity, high electrical conductivity, and the ability to tune their bandgaps through surface termination modifications [41,42]. $Ti_3C_2T_x$, the first member of the MXene family, remains the most widely studied due to its durability, the relatively straightforward process of etching aluminum layers from its MAX phase precursor, and outstanding physical and chemical characteristics [35,43,44]. Owing to their distinct physical and chemical properties, a variety of other MXene species have also been explored for different applications.

2.2. Synthesis of $Ti_3C_2T_x$ MXenes

Hydrofluoric acid (HF) etching was the first technique developed to transform MAX phases into MXenes[35]. Due to its simplicity and ability to produce high-quality MXenes [32], it remains one of the most widely used methods. However, this technique has notable drawbacks, primarily that HF is an extremely toxic and highly corrosive acid [45]. To reduce the risks associated with handling HF directly, alternative methods, such as in-situ HF generation via a reaction between LiF and HCl, were introduced. This approach also offers the added advantage of Li^+ cation intercalation between MXene layers [46]. A distinctive byproduct of the HF etching method is the formation of MXene layers with surface terminations, primarily -O, -OH, and -F. These functional groups provide an opportunity for surface engineering, enabling the electronic structure of MXene layers to be tuned by modifying the type and quantity of surface terminations[47]. Another modified etching method is the molten salt method that involves etching MAX phases by reacting them with a Lewis acidic molten salt at high temperatures [38]. Similar to the HF method, an intercalant is used; however, unlike HF etching, the molten salt method allows for the creation of diverse surface terminations during synthesis. For example, the electrochemical properties of $Ti_3C_2T_x$ electrodes in supercapacitors are degraded by the -F terminations produced by HF etching. To remedy this, Guo et al. [48] applied a one-step LiCl-KCl-K_2CO_3 molten salt etch and delaminate process to replace the -F terminations of $Ti_3C_2T_x$ with -O. Overall, the MXene saw a drop of -F content from 11.23 to 3.43 at% which precipitated an increase in specific capacity, capacitance retention, conductivity, and the electrochemical activity specific surface area.

The hydrothermal etching method was developed as a safer and more environmentally friendly alternative to the highly corrosive and hazardous HF etching process. This technique enables efficient exfoliation and the production of high-quality MXene flakes, offering the added advantages of larger interlayer spacing and improved delamination properties. The hydrothermal etching method utilizes high-pressure and high-temperature conditions in an aqueous MXene solution to produce high-purity multilayer MXenes [45]. For example, Peng et al. [32] employed this technique to synthesize $Ti_3C_2T_x$ MXenes by reacting their respective MAX phases with HCl and HCl+$NaBF_4$ solutions, followed by heating in an autoclave. The resulting MXenes were delaminated using DMSO and

 doi:10.20944/preprints202502.1240.v1

sonication. XRD analysis revealed that the hydrothermal method was significantly more effective at removing aluminum compared to the traditional HF etching method. Furthermore, dye adsorption studies with cationic MB and anionic MO showed that hydrothermally etched $Ti_3C_2T_x$ exhibited superior adsorption performance, with lower dye concentrations remaining compared to their non-hydrothermal counterparts. Some hydrothermal methods incorporate microwaves to excite reagents and reduce the temperature and time necessary for a reaction [49].

The resulting flakes were cleaned, delaminated using tetramethylammonium hydroxide, cleaned again, and then incorporated into a composite with reduced graphene oxide, which was effective at degrading dyes via photolysis [50]. A microwave hydrothermal ketal was utilized to rapidly create and oxidize $Ti_3C_2T_x$ Mxene nanosheets by Cao et al[49]. After cleaning, this $Ti_3C_2T_x$ was then combined with TiO_2 and CdZnS once more with the aid of a hydrothermal microwave in order to synthesize a synergetic photocatalytic semiconductive heterojunction that could degrade RhB dye molecules by 29.33% in under 90 min, which is 31.17-fold that of single Ti_3C_2 [51]. To significantly reduce etching time (from ~2−3 days to just 45 minutes) and eliminate -F terminations, Latif et al. [52] applied 5 to 30 M concentrations of NaOH etchant to Ti_3AlC_2 in a microwave hydrothermal reaction. Higher concentrations of NaOH saw the synthesized $Ti_3C_2T_x$ MXene achieve a 0.46% Al content under XRD and a semiconductive band gap energy of 1.30 to 1.60 eV.

3. Design and Fabrication of $Ti_3C_2T_x$ MXene-Based Hybrid Photocatalysts

$Ti_3C_2T_x$ MXene-based hybrid photocatalysts have been fabricated using various methods by integrating $Ti_3C_2T_x$ MXene nanosheets with a range of other nanomaterials. Some studies have shown that $TiO_2/Ti_3C_2T_x$ MXene composite photocatalysts can directly be prepared through the partial oxidation of $Ti_3C_2T_x$. Tran et al. [53] fabricated $TiO_2/Ti_3C_2T_x$ composites through an in-situ partial oxidation process, starting from $Ti_3C_2T_x$. This method led to the formation of microscale safflower-like structures composed of $TiO_2/Ti_3C_2T_x$ heterostructure nanorods. The transformation process was achieved via a sequential approach involving hydrothermal oxidation, alkalization, ion exchange, and heat treatment. Throughout these steps, the layered MXene flakes were broken into nanoparticles, from which $TiO_2/Ti_3C_2T_x$ nanorods grew radially. The resulting $TiO_2/Ti_3C_2T_x$ heterostructures exhibited exceptional photocatalytic properties. Their photocurrent was ten times higher than that of pristine MXene. Moreover, the photocatalytic degradation efficiency of RhB significantly improved, reaching 95%, compared to only 19% for MXene. Even after four cycles, the degradation efficiency remained above 95%, demonstrating excellent stability. The superior photocatalytic performance was attributed to the rapid generation of TiO_2 carriers, the suppressed recombination of charge carriers, and the enhanced light absorption provided by the porous safflower-like structure. Similarly, Quyen et al. [54] used a novel synthesis approach for TiO_2@ $Ti_3C_2T_x$ nanoflowers with a porous 3D framework derived from 2D $Ti_3C_2T_x$ MXenes via hydrothermal oxidation combined with a calcination process. This in situ transformation converts the initially conductive $Ti_3C_2T_x$ MXene into a semiconductor, forming a TiO_2@ $Ti_3C_2T_x$ heterojunction. As compared to 36% degradation rate of pure TiO_2 for RhB, the TiO_2@ $Ti_3C_2T_x$ composite exhibited an impressive 97% degradation within 40 minutes of light irradiation. This enhancement is attributed to the electronic structure of $Ti_3C_2T_x$, whose Fermi level is lower than that of TiO_2. Upon light excitation, photoinduced electrons transfer from the conduction band (CB) of TiO_2 to metallic $Ti_3C_2T_x$, leaving holes in the valence band (VB) of TiO_2. The resulting Schottky barrier at the interface suppresses electron diffusion back into TiO_2, thereby reducing electron-hole recombination and improving photocatalytic efficiency. Similarly, in situ solvothermal process has been used to prepare facet-exposed $TiO_2/Ti_3C_2T_x$ [55], since the exposed crystal plane of TiO_2 can effectively capture photogenerated holes and rapidly migrate to the surface of $Ti_3C_2T_x$, the photocatalytic performance towards methyl orange was significantly better as compared to the TiO_2 and $Ti_3C_2T_x$.

One of the simplest ways of preparing composites of $Ti_3C_2T_x$ MXene is calcination, in which the powders of two materials are heated at higher temperatures. In one example, [56] varying amounts of $Ti_3C_2T_x$ MXene powders were well-dispersed in a Zn^{2+} containing solution. The mixed solution was

 doi:10.20944/preprints202502.1240.v1

heated in an oven to evaporate the solvent. The powder was then calcined for 4 h at 550 °C with a heating rate of 5 °C/min in an ambient atmosphere to prepare ZnO/$Ti_3C_2T_x$ hybrid structures. The hybrid structure has reduced photoluminescence intensity, enhanced Brunauer-Emmett-Teller (BET) surface area, and better photocatalytic degradation efficiency for the degradation of MO and RhB as compared to the pristine ZnO.

The wet impregnation method, in which one material is deposited onto a solid support, can be used to prepare $Ti_3C_2T_x$ MXene composites. Nasri et al. [57] mixed powders of g-C_3N_4 and $Ti_3C_2T_x$ MXene in different proportions of weight and sonicated until the slurry was formed. The sample was then dried overnight at the temperature of 60ºC to obtain $Ti_3C_2T_x$ MXene/g-C_3N_4 composite photocatalyst. **Figure 1** summarizes the fabrication process of $Ti_3C_2T_x$ MXene/g-C_3N_4 composite photocatalyst. They found that 1 wt.% $Ti_3C_2T_x$ MXene/g-C_3N_4 heterostructure achieved higher photocatalytic activity for the degradation of methylene blue as compared to pure g-C_3N_4. This was attributed to intimate interfacial contact as seen by FESEM analysis, smooth transfer of photo charge carriers and larger BET surface area.

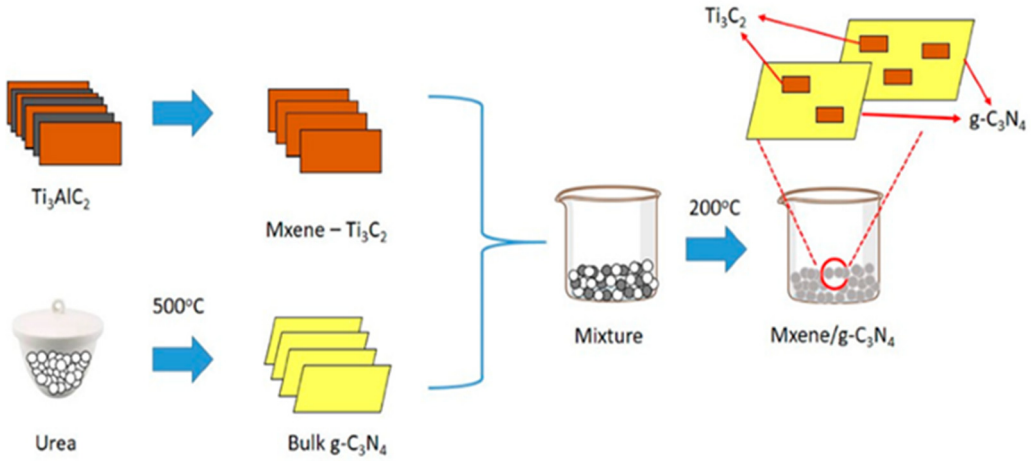

Figure 1. Schematic diagram of the $Ti_3C_2T_x$ MXene/g-C_3N_4 photocatalyst synthesis process. Adapted from Ref [57].

An electrostatically driven self-assembly strategy is one of the facile approaches to synthesizing MXene composites, especially in the solution. Cai et al.[58] have synthesized $Ag_3PO_4/Ti_3C_2T_x$ MXene Schottky catalyst with prominent photodegradation performance toward various organic dyes including methyl orange and 2,4-Dinitrophenol. In their work, $Ti_3C_2T_x$ sheets were first dispersed into DI water with the help of sonication, and $AgNO_3$ aqueous solution was added to the above $Ti_3C_2T_x$ suspension with vigorous stirring. Na_2HPO_4 aqueous solution was then added dropwise to the mixture with stirring for 2 h. The precipitate was washed with DI water several times and dried in a vacuum (80 °C) overnight before its use. The apparent rate constant of 2,4-Dinitrophenol degradation with $Ag_3PO_4/Ti_3C_2T_x$ was 2.5 times that of Ag_3PO_4/RGO and 10 times that of Ag_3PO_4. The enhanced photocatalysis activity of $Ag_3PO_4/Ti_3C_2T_x$ was attributed to the sufficient and close interfacial contact between Ag_3PO_4 and $Ti_3C_2T_x$, unidirectional electron flow to be trapped by the $Ti_3C_2T_x$ across the Schottky barrier, and the surface metal Ti sites on $Ti_3C_2T_x$ with stronger redox reactivity.

 doi:10.20944/preprints202502.1240.v1

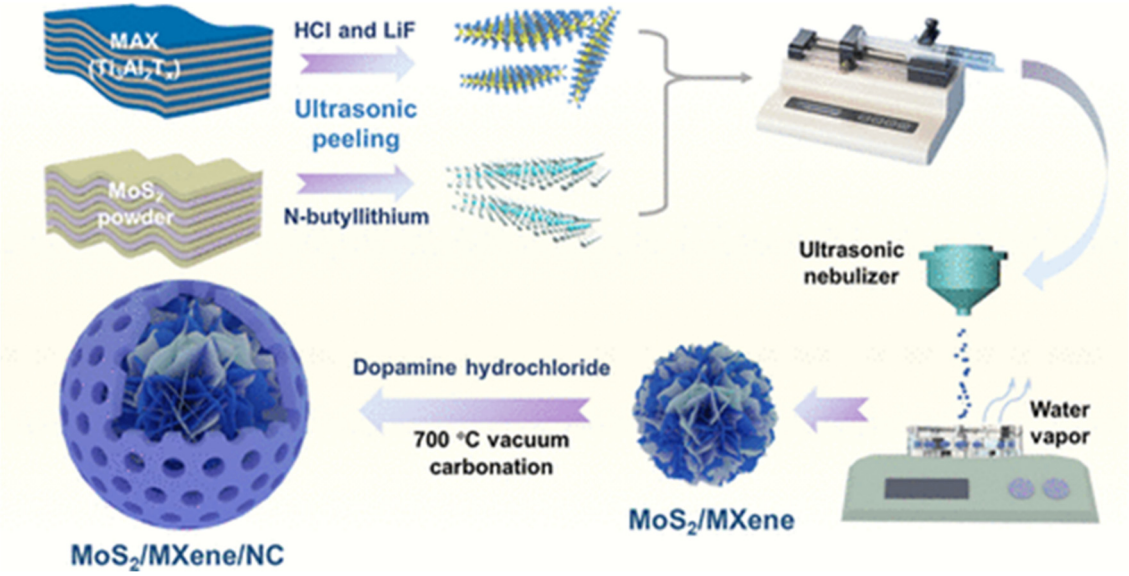

Figure 2. Synthesis and fabrication of $MoS_2/Ti_3C_2T_x$ MXene/N-doped carbon composite microspheres. Adapted from Ref[59].

Ultrasonic forces have been utilized in the fabrication of $Ti_3C_2T_x$ MXene-based composites to disrupt electrostatic attractions and van der Waals interactions. For example, Lee et al.[60] prepared the composites with heterojunctions of 2D/2D $WO_3/Ti_3C_2T_x$. The WO_3 nanosheets were dispersed in DI water, followed by the addition of varying amounts of $Ti_3C_2T_x$ nanosheets. The resulting suspension was subjected to sonication, where cavitation bubbles generated localized high-temperature and high-pressure spots, facilitating physical and chemical interactions between WO_3 and $Ti_3C_2T_x$. This process enabled the effective integration of WO_3 nanosheets with $Ti_3C_2T_x$ structures. The final suspension was then dried at 100 °C for 12 hours in an electric oven. The $WO_3/Ti_3C_2T_x$ heterojunction demonstrated significantly higher photoexcited carrier transfer and separation efficiency, leading to exceptional photocatalytic performance in MB degradation under visible light. Furthermore, the photoelectrochemical analysis of $WO_3/Ti_3C_2T_x$ revealed improved charge carrier mobility, effectively reducing the carrier transport barrier between WO_3 and $Ti_3C_2T_x$. A similar approach has been used to synthesize $Ti_3C_2T_x/CuFe_2O_4$ nanohybrids[61]. A similar process has been used to prepare ZnS nanoparticles/layered MXene sheets[62]. Similarly, manganese oxide decorated 2D $Ti_3C_2T_x$ MXene containing MnO_2 nanopetals was also synthesized using the ultrasonic approach [63]. The synergistic effect of these two nanomaterials inhibited the electron/hole pair recombination and improved the surface activity. The nanocomposite showed high photocatalytic ability to methylene blue as about 99% of the methylene blue degraded within 30 minutes.

The sol-gel method uses metal alkoxide precursors to form gels through hydrolysis, usually at lower temperatures, followed by calcination. For example, Iqbal et al. [64] used the double-solvent solvothermal method to prepare $BiFeO_3$ (BFO)/$Ti_3C_2T_x$ nanohybrid. In their work, $Ti_3C_2T_x$ MXene in DI water and the BFO nanoparticles in a mixture of acetic acid and ethylene glycol were ultrasonicated separately. Both solutions were then mixed and transferred to a Teflon-lined steel autoclave for solvothermal synthesis in which the mixture was heated at 160 ° C for 2 h. The final product was washed and then dried at 80 ° C for 3 h. The nanohybrid was found to have a high BET surface area of 147 m2 g^{-1}, a low band gap of 1.96 eV, and a low recombination time. These properties led to a superior photocatalytic activity for Congo red as it was able to degrade Congo red only in 42 mins under visible light irradiation. A similar process was used to prepare La- and Mn-co-doped BFO nanoparticles embedded in $Ti_3C_2T_x$ sheets [65].

The solvothermal process, in which reactions occur in a solvent under elevated temperature and pressure within a sealed system, has also been used to synthesize nanocomposites of MXene. This method has been used by W Zheng et al.[66] to synthesize $SnO_2/Ti_3C_2T_x$ composites and by Zhou et al.[67] to prepare $CeO_2/Ti_3C_2T_x$ nanocomposites from CeO_2 nano-rods on $Ti_3C_2T_x$ sheets. The

 doi:10.20944/preprints202502.1240.v1

nanocomposites exhibited enhanced photocatalytic activity for the photodegradation of Rhodamine B under UV-light irradiation as compared to pure CeO_2 semiconductors and $Ti_3C_2T_x$. The enhancement of photocatalytic activity was attributed to the narrow band energy in the composite as compared to CeO_2, which enhanced utilization of solar energy, both exhibiting high efficiency in pollutant degradation [67]. Similar process has been used to prepare $BiVO_4/Ti_3C_2T_x$ nanocomposite [68].

In another study [69], $Ti_3C_2T_x$ powder was added to the ultrasonicated precursor solution of MoS_2. The mixture was heated at 200 °C for 10 hours, then cooled, centrifuged, washed with deionized water, and dried to produce the $MoS_2@Ti_3C_2T_x$ nanohybrid in **Figure 2**. The authors found that the Schottky junction and heterojunction between $Ti_3C_2T_x$ and MoS_2 were instrumental in prolonging the recombination time of electron-hole pairs and widening the absorption range of visible light. As a result, nanohybrid showed higher photocatalytic activity towards methyl orange. Also, $TiO_2/Ti_3C_2T_x$ MXene was prepared through a hydrothermal reaction of nano-TiO_2 and $Ti_3C_2T_x$ MXene nanosheets [70]. The higher photocatalytic activity was attributed to the inhibition of electron-hole recombination, which promoted the accumulation of electrons and easier electron transfer from TiO_2 to MXene. Similarly, $AgNPs/TiO_2/Ti_3C_2T_x$ composite was prepared by hydrothermal treatment of $Ti_3C_2T_x$ nanosheets and $AgNO_3$ salt at 160 °C for 12 h with the heat ramp-up of 2 °C/min [71]. They found that the photocatalytic performance of oxidized form improved significantly as compared to the pristine form. Also, superior degradation efficiency for MB and RhB was achieved for $AgNPs/TiO_2/Ti_3C_2T_x$ as compared to pristine MXene. A similar process has been used to prepare $Bi_2WO_6/Ti_3C_2T_x$ by heating layered $Ti_3C_2T_x$ MXene and $Bi(NO_3)_3.5H_2O$ at 160 ºC for 16 h.

4. Photocatalytic Degradation of Dyes Using $Ti_3C_2T_x$ MXene Hybrids

Photocatalysis is a relatively safer and low-cost strategy for degrading hazardous organic pollutants[72–74]. $Ti_3C_2T_x$ MXene, with its unique lamellar structure and remarkably high metallic conductivity, and excellent hydrophilicity has emerged as a promising member of MXene family. Its distinctive properties have enabled its use as a photocatalyst for environmental remediation [75,76] and co-catalyst for enhancing the photocatalytic degradation potential of composite photocatalysts[77,78]. $Ti_3C_2T_x$ MXene-based hybrid photocatalysts have several advantages, like improved charge separation, sufficient atomic utilization, tunable bandgap, improved morphology, increased electron transfer efficiency, and improved photocatalytic activity[79–81]. We assess the effectiveness of $Ti_3C_2T_x$ MXene-based hybrid photocatalysts by comparing them to non-hybrid photocatalysts in the degradation of both cationic and anionic dyes.

Table 1. Selected nonhybrid photocatalysts with photocatalytic degradation performance towards cationic and anionic dyes.

Nonhybrid photocatalysts	Dyes	Type of dyes	Degradation percentage (%)	References
CdS	MO	Anionic	95 (300 min)	Ref[81].
δ-Bi_2O_3	MO	″	98 (180 min)	Ref[82].
TiO_2 NPs	MO	″	~95 (~120 min)	Ref[83].
ZnO	MB	Cationic	40.88 (21h)	Ref[84].
TiO_2 Hollow Nanofiber	MB	″	95.2 (4h)	Ref[85].
CuO	MB	″	62 (270 min)	Ref[86].
$Bi_2S_2O_3$	CR	Anionic	82 (75 min)	Ref[87].
ZnO	CR	″	97.6(75 min)	Ref[88].
$MoSe_2$	CR	″	8.44(120 min)	Ref[89].
g-C_3N_4	RhB	Cationic	75 (180 min)	Ref[90].
$BiMnO_3$	RhB	″	68 (75 min)	Ref[91].

 doi:10.20944/preprints202502.1240.v1

Table 1. Summarizes the results on the studies of photocatalytic degradation of anionic dyes such as MO, and CR and cationic dyes, MB and RhB. Dey and Ratan Das [81] utilized CdS as a nonhybrid photocatalyst, achieving 95% degradation of MO within 300 minutes. Additionally, they employed ZnO to degrade CR, achieving 97.7% degradation in 75 minutes.[88]. In a separate study, N. N. Mohammad Jafri et al. [85] utilized TiO_2 nanofibers, achieving 95.2% degradation of the cationic dye, MB, within 240 minutes. Similarly, S. Fang et al.[90] prepared g-C_3N_4 to degrade RhB, achieving 75% degradation in 180 minutes. Additionally, the ZnO standalone photocatalyst required 21 hours (1260 minutes) to degrade 40.88% of MB [84] and while $MoSe_2$ took 2 hours (120 minutes) to achieve only 8.44% degradation [89]. Such prolonged durations and low efficiencies make these photocatalytic processes economically and time inefficient for the practical degradation of organic dye pollutants. Furthermore, pristine MXene photocatalysts demonstrate lower dye degradation efficiency. For instance, J. Qu et al. [115] reported that alkalized $Ti_3C_2T_x$ exhibited reduced photocatalytic performance compared to $Ti_3C_2T_x$ MXene-based hybrid photocatalysts. The alkalized $Ti_3C_2T_x$ achieved degradation rates of only 17.3% for the cationic dye, RhB and 2.8% for the anionic dye, MO within 120 minutes.

On the other hand, $Ti_3C_2T_x$ MXene-based hybrid photocatalysts have shown remarkable potential for degrading both cationic and anionic dyes under light irradiation. For example, a $Ti_3C_2T_x$ MXene-based hybrid photocatalyst achieved a degradation efficiency of 99.7% for MO and 100% for RhB, as detailed in **Table 2**. These photocatalysts effectively break down dye molecules into less harmful degradation products, showcasing their efficiency in addressing organic dye pollutants. Such high efficiency can be attributed to the rich surface chemistry, tunable bandgap structures, high electrical conductivity, hydrophilicity, thermal stability, and large specific surface area with abundant active sites. These properties facilitate efficient dye adsorption and subsequent photocatalytic degradation. For instance, M.S.I. Nasri et al. [6] reported a 100% degradation efficiency for MB using a $Ti_3C_2T_x$/g-C_3N_4 hybrid within 180 minutes. This remarkable performance was linked to the effective charge separation and transfer capabilities of $Ti_3C_2T_x$ MXene, which significantly enhanced the generation of reactive species essential for dye degradation.

Q.T.H. Ta et al. [56] demonstrated that ZnO/$Ti_3C_2T_x$ achieved a degradation efficiency of 99.7% for MO, while RhB was effectively degraded by Bi_2WO_6/$Ti_3C_2T_x$ with an impressive efficiency of 99.9% within 20 minutes. Similarly, Danxia Zhao and Chun Cai [92] reported comparable results (refer to Table 2 for details). This study highlights the pivotal role of MXene incorporated heterostructure, characterized by its high conductivity and ability to facilitate rapid electron transfer, which are essential for efficient photocatalysis [93]. For instance, Jun Yao and Chaoxia Wang [94] demonstrated that MB achieved a degradation efficiency of 93.3% within 160 minutes using a catalyst-to-dye ratio of 1.5:1 with standalone catalyst, TiO_2. However, the MXene-based hybrid $AgNP_s$/TiO_2/$Ti_3C_2T_x$ achieved 99% degradation in just 30 minutes with a 2.5:1 catalyst-to-dye ratio, demonstrating superior efficiency in both time and degradation rate compared to non-hybrid photocatalysts [95].

$Ti_3C_2T_x$ MXene-based hybrid represents a versatile and highly effective class of photocatalysts for the degradation of both anionic and cationic dyes, making them suitable for various environmental remediation applications. For example, $Ti_3C_2T_x$ MXene-based nanocomposites prepared with Mn_2O_3 were evaluated for photocatalytic dye degradation under light, demonstrating efficient photocatalysis. The 1D Mn_2O_3-$Ti_3C_2T_x$ (20 wt%) nanocomposite achieved 100% degradation of MB within 25 minutes, effectively removing the dye[96], Similarly, $NiMnO_3$/$NiMn_2O_4$-$Ti_3C_2T_x$ MXene nanocomposites achieved 100% degradation of MB in 50 minutes, showcasing excellent dye removal efficiency[97]. Wang et al. [98] synthesized $Ti_3C_2T_x$/$Bi_4Ti_3O_{12}$ heterojunction via a facile in-situ solvothermal method, demonstrating exceptional visible-light-driven photocatalytic performance by achieving 100% degradation of MO and RhB within 60 and 50 minutes, respectively (see details in Table 2). This result highlights the potential of $Ti_3C_2T_x$ MXene-based hierarchical composites for water remediation, offering a sustainable approach for the degradation of anionic and cationic organic pollutant applications. In an independent study, Iqbal et al. [64] reported that the

 doi:10.20944/preprints202502.1240.v1

BFO/$Ti_3C_2T_x$ MXene hybrid achieved 100% degradation of CR in 42 minutes, highlighting its potential for photocatalysis applications.

While we observed that factors such as the synthesis method, pH, catalyst-to-dye ratio, concentration, and structure significantly influence the functionality and effectiveness of photocatalysts, we conclude from this evaluation that $Ti_3C_2T_x$ MXene-based hybrid photocatalysts exhibit superior photocatalytic performance and efficiency in the degradation of organic pollutant dyes compared to nonhybrid photocatalysts.

Table 2. $Ti_3C_2T_x$ MXene-based hybrid photocatalysts with photocatalytic degradation performance towards cationic and anionic dyes.

MXene-based hybrid photocatalysts	Dyes	Type of dyes (Based on charge)	Degradation Percentage/ (Time)	References
$TiO_2/Ti_3C_2T_x$	MO	Anionic	92(50 min)	Ref.[55]
$MoS_2@Ti_3C_2$	MO	Anionic	98(60 min)	Ref.[69]
$Ti_3C_2/TiO_2/CuO$	MO	Anionic	99 (80 min)	Ref.[99]
$ZnO/Ti_3C_2T_x$	MO	Anionic	99.7(50	Ref.[56]
$Ti_3C_2T_x$ /$Bi_4Ti_3O_{12}$	MO	Anionic	100(60 min)	Ref[98]
TiO_2/Ti_3C_2 Mxene	MB	Cationic	96.44(60)	Ref[100]
$AgNP_s/TiO_2/Ti_3C_2T_x$	MB	Cationic	99 (30 min)	Ref[95]
$Ti_3C_2/g\text{-}C_3N_4$	MB	Cationic	100(180 min)	Ref[101]
$NiMnO_3/NiMn_2O_4$ - $Ti_3C_2T_x$ MXene	MB	Cationic	100 (50 min)	Ref[97]
1D Mn_2O_3-$Ti_3C_2T_x$	MB	Cationic	100(25 min)	Ref [96]
Mn-codoped bismuth ferrite/Ti_3C_2	CR	Anionic	93(30 min)	Ref[65]
$CoFe_2O_4$ @MXene	CR	Anionic	98.9(30 min)	Ref[102]
$BiVO_4/Ti_3C_2$	CR	Anionic	99.5(60 min)	Ref[68]
BGFO-20Sn/MXene	CR	Anionic	100(120 min)	Ref[103]
$BiFeO_3/Ti_3C_2$	CR	Anionic	100(42min)	Ref[64]
$TiO_2@Ti_3C_2$	RhB	Cationic	97(40 min)	Ref[54]
BiOBr/TiO_2/ $Ti_3C_2T_x$	RhB	Cationic	99.8(30 min)	Ref[104]
Bi_2WO_6/Ti_3C_2	RhB	Cationic	99.9(20 min)	Ref[92]
ZnS/MXene	RhB	Cationic	100(100 min)	Ref [105]
$Ti_3C_2T_x/Bi_4Ti_3O_{12}$	RhB	Cationic	100 (50 min)	Ref [98]

5. Computational Studies and Simulations

The investigation of $Ti_3C_2T_x$ MXene-based hybrids for photocatalytic applications benefit significantly from computational tools and techniques. These methods complement experimental approaches by providing insights into atomic-level phenomena, guiding material design, and predicting performance under varying conditions.

Chen et al.[106] investigated the electronic and optical properties of -F terminated, -O terminated, and termination-free Ti_3C_2 in a MXene nanosheet/TiO_2 composite using Density Functional Theory (DFT). Their study revealed that surface terminations reduced the density of electronic states, lowered conductivity, and enhanced stability compared to the termination-free MXene. DFT analysis also demonstrated the feasibility of electron transfer from TiO_2 to Ti_3C_2 and identified the Schottky barrier at the interface between the two materials. Furthermore, the computational modeling highlighted the synergy between the composite components, showing an extended range of light absorption, suppressed electron-hole recombination, and improved hole oxidation efficiency in the valence band of TiO_2. These factors significantly enhanced the photocatalytic performance of the Ti_3C_2/TiO_2 composite, making it a highly promising candidate for

 doi:10.20944/preprints202502.1240.v1

photocatalytic applications, such as treating organic pollutants like dye molecules[106]. Lemos et al. utilized a computational model to evaluate the performance of a $Ti_3C_2T_x/TiO_2$ nanocomposite hybrid for use in photocatalyzed dye-sensitized solar cells. Through DFT calculations, they discovered that the anatase potential is reduced at the nanocomposite interface and that the nanocomposite exhibits improved photocarrier separation at the interface between the nanocomposite and the dye[107]. Furthermore, Yang et al[108]. conducted computational analysis to confirm that a transition metal dichalcogenide/MXene photocatalyst hybrid, MoS_2/Ti_3C_2, functions as a Schottky barrier. A Bader charge analysis revealed that the difference in work functions between MoS_2 and Ti_3C_2, combined with a built-in electric field, facilitates the transfer of photogenerated electrons from MoS_2 to the Ti_3C_2 electron sink. This efficient electron transfer enhances photocarrier separation, resulting in longer-lasting photogenerated holes and exceptional photodegradation performance against rhodamine B dye in wastewater[108].

Several more computational techniques have been employed to assess and optimize the photocatalytic mechanisms in the MXene-based composites for dye degradation applications. Liu et al[109] developed a $g\text{-}C_3N_4/Ti_3C_2$ (CNTC) heterojunction by hybridizing 2D Ti_3C_2 MXene with 3D $g\text{-}C_3N_4$ for enhanced photodegradation of RhB dye. This photocatalyst exhibited a high specific surface area (85.08 m^2/g) and remarkable charge migration capabilities. To evaluate its improved photocatalytic performance, the researchers utilized DFT analysis to examine the differential charge density, electron distribution, and charge transfer dynamics between $g\text{-}C_3N_4$ and the Ti_3C_2 sink. The study revealed that the excellent conductivity of Ti_3C_2 stemmed from the overlap between the Fermi level and conduction band in the heterojunction. This led to an understanding that these 2D/3D heterojunctions significantly promote charge transfer and separation, which are essential for efficient photocatalysis. Additionally, the combination of a high specific surface area and abundant active sites makes the CNTC particularly effective for dye photodegradation[109]. Cheng et al[110]. synthesized a self-cleaning BiOCl-polypyrrole (PPy)@$Ti_3C_2T_x$ MXene composite membrane with excellent photocatalytic activity and high flux, designed for filtering and degrading pollutants. The membrane's performance was tested against various dyes. To gain deeper insight into the photocatalytic mechanisms, particularly charge separation and degradation, the researchers conducted DFT calculations. Density of States (DOS) simulations revealed that the chemisorption of oxygen into vacancies on the BiOCl surface generated superoxide radicals. These radicals enhanced the composite's photocatalytic efficiency through redox interactions with dye molecules and other pollutants [110]. Wang et al. [111] synthesized an S-scheme Pt-$MnO_2/TiO_2@Ti_3C_2T_x$ composite using an electrostatically self-assembled Ti-O-Mn bond and evaluated its oxidative photodegradation performance against MB, MO, and RhB dyes. To investigate the photocatalytic mechanisms, DFT calculations were performed, revealing that the Ti-O-Mn bond induced the formation of metastable Ti atoms and electrostatically adsorbed Mn^{2+} ions. This bond facilitated the separation of photoinduced carriers and optimized their transport pathways. Additionally, the DFT analysis identified the formation of S-scheme heterojunctions between MnO_2 and TiO_2 through the Ti-O-Mn bond, driving the flow of photogenerated carriers. These factors collectively enhanced the composite's photocatalytic efficiency [111].

Density Functional Theory (DFT) has been employed in conjunction with the Finite Element Method to explore ways to enhance the photocatalytic activity and membrane permeability of a novel MXene-based composite membrane, N-doped $Bi_2O_2CO_3@Ti_3C_2T_x$/Polyethersulfone, designed for oil/water separation and dye degradation[112]. Through DFT analysis of the electron distribution and band structure of doped versus undoped $Bi_2O_2CO_3$, they found that N doping improved conductivity, enhanced electron transition activity, and facilitated photogenerated carrier transport (attributed to valence band dispersion), making $Bi_2O_2CO_3@Ti_3C_2T_x$/Polyethersulfone more effective for photocatalytic applications [112].

 doi:10.20944/preprints202502.1240.v1

6. Other Applications of $Ti_3C_2T_x$ MXene-Based Hybrid Photocatalysts

Beyond organic dye degradation, $Ti_3C_2T_x$ MXene-based hybrid photocatalysts have demonstrated potential for various other applications. They have shown considerable promise in wastewater treatment, especially in degrading organic pollutants such as dyes, pharmaceuticals, and pesticides. Composite materials of $Ti_3C_2T_x$ MXene with semiconductors such as TiO_2 or ZnO have shown even greater photocatalytic efficiencies; the synergy between MXenes and these semiconductors results in improved light absorption and charge separation [113,114]. For instance, $Ti_3C_2T_x/TiO_2$ composites exhibit enhanced photocatalytic activity under visible light due to the synergistic effects of both materials. These composites can efficiently degrade different dyes under sunlight, including RhB and MO, making them suitable for sustainable and cost-effective wastewater treatment [115]. Furthermore, doping MXenes with other elements or combining them with carbon-based materials like graphene can further enhance their photocatalytic properties. Nitrogen-doped $Ti_3C_2T_x$ MXene shows improved photocatalytic degradation of antibiotics such as tetracycline under visible light, highlighting their potential in treating pharmaceutical contaminants in wastewater[116]. $Ti_3C_2T_x$ MXene-based hybrid photocatalysts are also being explored for air purification applications, particularly in removing volatile organic compounds (VOCs) and other airborne pollutants. $Ti_3C_2T_x$ MXene, when combined with photocatalysts like TiO_2, can effectively degrade formaldehyde and toluene, common indoor air pollutants, under UV and visible light[117]. Incorporating noble metals like Au or Ag onto $Ti_3C_2T_x$ MXene can further enhance their photocatalytic performance by creating localized surface plasmon resonance, increasing light absorption, and improving the degradation rates of VOCs [118]. Additionally, Z-scheme heterostructures involving $Ti_3C_2T_x$ MXene have been developed to mimic natural photosynthesis, achieving efficient separation and transfer of photogenerated charge carriers and enhancing photocatalytic degradation of air pollutants [119]. The most applied technology is the $Ti_3C_2T_x$ MXene-based TiO_2 photocatalyst, which utilizes photocatalysis for glass cleaning, where UV or visible light activates TiO_2, generating reactive oxygen species that decompose organic pollutants on the glass surface. This self-cleaning mechanism maintains transparency, reduces manual cleaning, and prevents pollutant buildup, enhancing the efficiency and durability of glass surfaces.

Beyond the degradation of dyes, the degradation of other organic pollutants, such as pharmaceutical waste and VOCs, has appeared as a challenging task that needs immediate attention[120]. In recent years, extensive studies[121] reported photocatalysis as an attractive method for the efficient degradation of organic pollutants. Properties such as surface-to-volume ratio, light interaction and mechanical stability define the photocatalytic performance of a catalyst [122]. Among the variety of materials reported so far, $Ti_3C_2T_x$ MXenes gained significant attention as a photocatalytic material [123]. Further, the integration of $Ti_3C_2T_x$ MXenes with other nanomaterials can significantly improve photocatalytic performance[124].

Kumar et al. [125] reported a novel photocatalyst with a composition of g-C_3N_4, $Ti_3C_2T_x$ and Au nanoparticles for the degradation of cefixime. **Figure 3**a shows the degradation mechanism of cefixime decomposition under light. The composition with 3 wt% $Ti_3C_2T_x$ shows the highest degradation up to 64.69% cefixime in 105 min using visible light irradiation as shown in **Figure 3**b and c. Similarly, Diao et al. [126] reported an efficient photocatalytic degradation of tetracycline hydrochloride using MXene-based photocatalysts comprising g-$C_3N_4/Ti_3C_2T_x/TiO_2$. The reported ternary catalysts show superior performance, chemical and photostability with recyclability. Another MXene-based ternary photocatalyst reported by Zhou et al.[127] for photocatalytic degradation of enoxacin under visible light where $Ti_3C_2T_x$ helps to improve charge separation at the interface and hence efficient degradation. Rdewi et al. [128] reported a ZnO-TiO_2-MXene photocatalyst for the decomposition of carbamazepine molecules in wastewater under solar irradiation. The presented results show 99.6% removal efficiency at a pH of 7 as a result of improved charge carrier transport and reduced recombination rate due to the incorporation of TiO_2-MXene with ZnO photocatalysts. The excellent photocatalytic performance also shows the reusability for multiple decomposition cycles with exceptional efficiency. Similarly, Abbas et al. [129] reported a ZnO-TiO_2-MXene

 doi:10.20944/preprints202502.1240.v1

photocatalyst for the decomposition of ceftriaxone sodium molecules in water using simulated solar light.

Furthermore, Sukidpaneenid et al. [130] reported $Ti_3C_2T_x/TiO_2$ photocatalysts for the degradation of enrofloxacin antibiotics in water. The excellent control over TiO_2 amount on MX by varying hydrothermal processes played a crucial role in tuning photocatalytic properties. Further, the intercalation of sodium ions significantly improved the adsorption, and the synergetic effect of TiO_2 amount and NaCl treatment led to the efficient removal of enrofloxacin. Shahzad et al. [131] demonstrated the degradation of carbamazepine (CBZ) under direct sunlight and UV light using $Ti_3C_2T_x$-based heterostructure photocatalysts with {001} TiO_2. The results show Kapp value under UV irradiation was higher than under sunlight for degradation CBZ also, the effects of pH on degradation performance were taken into account. Mohanty et al.[132] reported a series of $SrTiO_3/Ti_3C_2T_x$-based photocatalysts decorated with Au nanoparticles for the degradation of colorless organic pollutants such as ciprofloxacin under sunlight. The significant enhancement in photocatalytic degradation for the plasmon-mediated heterostructure catalysts is attributed to the absorption of broad solar spectrum, charge separation and charge transport. Du et al. [133] demonstrated the photocatalytic degradation of tetracycline using CeO_2-$Ti_3C_2T_x$-TiO_2 (CeMXT). The composite shows an excellent degradation efficiency of 94.70% for 22.19 mg/L in 104.13 minutes with 0.65 g/L of catalysts with a pH of 4.72. This excellent degradation efficiency is attributed to increased radical generation and charge separation.

Sergi et al. [134] . reported a series of TiO_2-$Ti_3C_2T_x$ MXene photocatalysts with controlled composition for the realization of improved photocatalytic removal of benzene. The incorporation of TiO_2 with $Ti_3C_2T_x$ MXene improved the optical absorption to enhance the photocatalytic performance. The report showed the potential of $Ti_3C_2T_x$ MXenes for the removal of VOCs and heterostructure to enhance the photocatalysis performance. Further, Huang et al.[117] reported the degradation of HCHO (formaldehyde) and CH_3COCH_3 (acetone) using Bi_2WO_6/Ti_3C_2 (BT4) under light. Bi_2WO_6 as photocatalysts suffers from a high recombination rate, and combination with Ti_3C_2 can significantly improve the charge separation. Ti_3C_2 led charge separation caused charge transfer at the interface, significantly improving the photocatalytic performance of BT4. Further, the higher adsorption of formaldehyde and acetone at the Ti_3C_2 surface than at the surface of Bi_2WO_6 estimated from DFT simulation, synergistically tunes photocatalytic performance. By value, the degradation of formaldehyde and acetone for Bi_2WO_6 was 2 and 6.6 times higher for BT4, respectively. Mo et al.[135] demonstrated photocatalytic and photothermal removal of VOCs (phenol) from water using $TiO_2/Ti_3C_2T_x/C_3N_4$/PVA (TTCP) hydrogel under sunlight. **Figure 3**d shows the SEM image of TTCP. The VOC removal efficiency varies from 69.4% to 100% at different concentrations of phenol (1-50 mg/L) shown in **Figure 3**e and f. The membrane significantly lowers the TDS and TOC. The TDS level was reduced by more than 100 times magnitude, and TOC removal efficiency was observed to be 80%.

 doi:10.20944/preprints202502.1240.v1

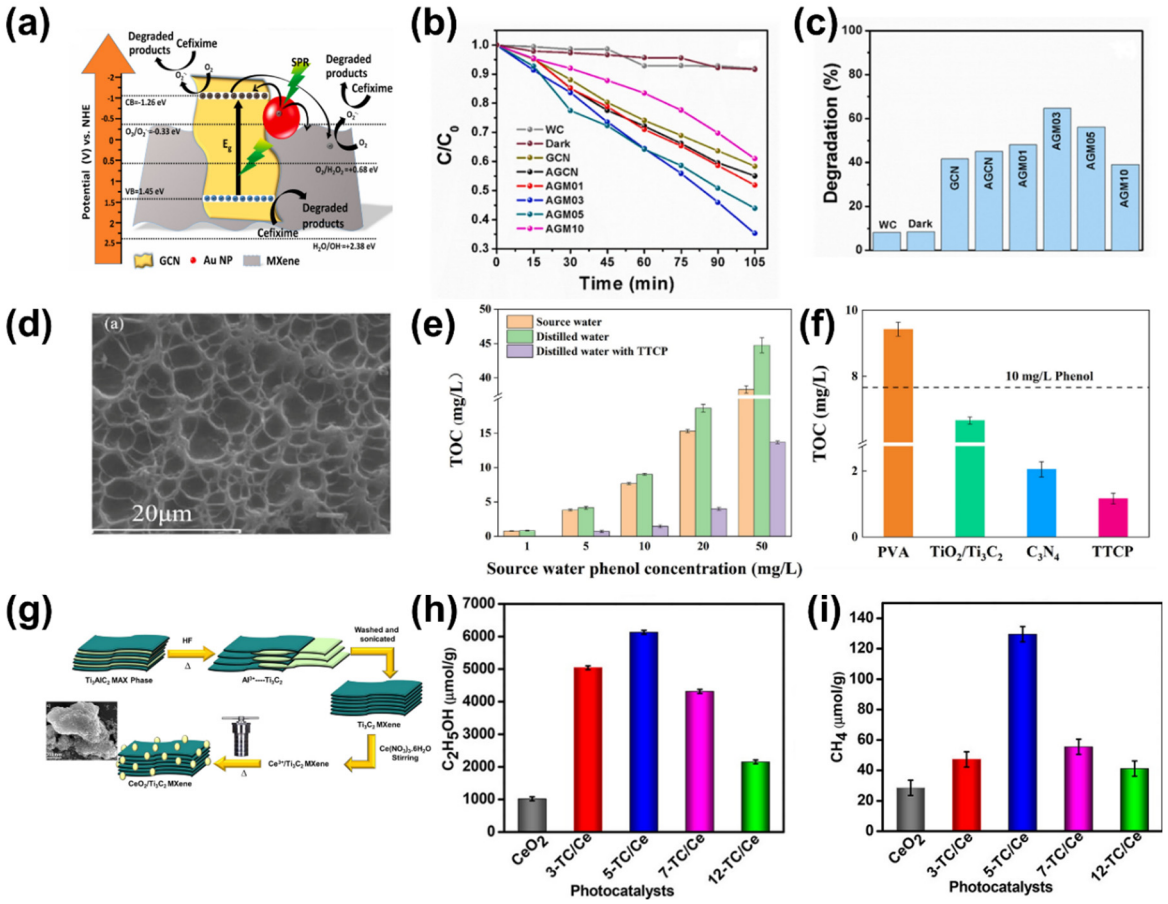

Figure 3. (a) Schematic representation of cefixime degradation mechanism under light. (b) Degradation kinetics of cefixime degradation (c) Histogram representation of degradation rate (%).[125] (d) SEM image of the TTCP hydrogel (e) TOC of source water under different phenol concentrations (orange column), distilled water without photocatalyst (green column) and distilled water with TTCP hydrogel (violet column). (f) TOC of distilled water with different catalysts.[135] (g) Schematic illustration of the synthesis process of the $Ti_3C_2T_x$ MXene/CeO_2 photocatalysts (inset SEM image). Comparative representation of the production of (h) C2H5OH and (i) CH_4 under solar light illumination with different catalysts. [136].

The reduction of CO_2 using photocatalytic activity is another aspect of environmental remediation applications. Reducing CO_2 into other useful byproducts using light-activated catalysts shows the futuristic pathway towards sustainability [90]. The excellent charge separation and slow recombination rate show the potential of $Ti_3C_2T_x$ MXene as a catalytic material for CO_2 reduction[137]. In this regard, Cao et al.[138] demonstrated 2D/2D ultrathin $Ti_3C_2T_x/Bi_2WO_6$ nanosheets prepared by in situ growth of Bi_2WO_6 nanosheets over $Ti_3C_2T_x$ nanosheets. The proposed hybrid catalyst shows improved efficiency towards reduction of CO_2 under light due to reduced charge transfer distance, improved surface-to-volume ratio, and adsorption sites. The hybrid catalyst shows improved production of CH_4 and CH_3OH compared to Bi_2WO_6. Quantitatively, the production of CH_4 increased from 0.41 μmol g-1 h-1 to 1.78 μmol g-1 h-1, while the production of CH_3OH increased from 0.07 μmol g-1 h^{-1} to 0.58 μmol g-1 h-1. Similarly, Mishra et al.[136] investigated a $Ti_3C_2T_x$-CeO_2 hybrid catalyst with varying ratios of $Ti_3C_2T_x$ for the photocatalytic reduction of CO_2. The schematic synthesis process for hybrid catalysts shown in **Figure 3**g. Surprisingly, the hybrid catalyst with 5 wt% $Ti_3C_2T_x/CeO_2$ shows a production of 6127.04 μmol g^{-1} for ethanol and 129.5 μmol g^{-1} for methane, way higher than CeO_2 within 5 hr of time as shown in **Figure 3**h and i. Another report by Li et al. [139] shows the potential of Ti_3C_2 based hybrid catalyst comprising g-C_3N_4/ZnO/$Ti_3C_2T_x$ for the reduction of CO_2 in methane (CH_4) and carbon monoxide (CO). The hybrid framework shows a notably higher production rate of 1.41 μmol $g^{-1}h^{-1}$ towards CO increased by a factor of 2.7 and 1.7 as that of ZnO and g-C_3N_4.

 doi:10.20944/preprints202502.1240.v1

As the literature suggests, $Ti_3C_2T_x$ MXene has been extensively studied in recent years for its wide range of photocatalytic uses in environmental applications. The results reported so far show the potential of $Ti_3C_2T_x$ MXene-based catalysts for the degradation of dyes, pharmaceutical wastes, VOCs along with CO_2 reduction. The higher surface ratio, charge separation at the interface and excellent absorption of light plays significant roles in the photocatalytic performance of these photocatalysts.

7. Working Mechanism of $Ti_3C_2T_x$ MXene-Based Hybrid Photocatalyst

The electronic structure of $Ti_3C_2T_x$ MXene-based photocatalysts plays a crucial role in their ability to degrade targeted pollutants through photocatalysis. In general, an ideal photocatalyst should possess a suitable bandgap, strong absorption in the visible range, prolonged charge separation lifetimes, and adequate redox potential [105]. To enhance the efficiency of photocatalysis, co-catalysts are employed to separate photogenerated charge carriers. When materials such as ZnO, CdS, TiO_2, and Ti_3C_2 are used as co-catalysts, Schottky junctions formed with $Ti_3C_2T_x$ facilitate the rapid dissociation of these charge carriers [140]. As discussed in the previous section, $Ti_3C_2T_x$ MXene-based photocatalyst composites demonstrate superior photocatalytic performance compared to non-hybrid photocatalysts. This is attributed to the abundant active sites available on $Ti_3C_2T_x$ MXene-based hybrids, enhanced bandgap, improved light-harvesting capability, reduced charge carrier recombination, and extended photoelectron lifetime [141].

During photocatalytic degradation, $Ti_3C_2T_x$ MXene-based hybrid photocatalysts absorb visible light, causing photogenerated electrons to become excited into the CB while leaving holes in the VB [20]. The excited charge carriers are then transferred to the $Ti_3C_2T_x$ MXenes at the interface, primarily due to the higher potential of $Ti_3C_2T_x$ MXene. Photogenerated electrons from the $Ti_3C_2T_x$ MXenes migrate to the surface and react with O_2 to produce superoxide radicals ($\bullet O^{2-}$), and holes from the TiO_2 react with hydroxyl ions to produce hydroxyl radicals (OH). These radicals cause the degradation of cationic and anionic dyes of organic pollutants [20,142,143].

A photocatalytic mechanism of $Ti_3C_2T_x$–TiO_2 hybrid for anionic dye (e.g., MO) degradation has been presented in **Figure 4**a as an example. Initially, the light source provides high-energy photons, which activate the TiO_2 component, generating photoinduced electrons (e^-) in its CB and leaving holes (h^+) in its VB. The photoelectrons rapidly migrate from the CB of TiO_2 to the $Ti_3C_2T_x$ MXene, facilitated by its high electrical conductivity [95,144]. As a result, $Ti_3C_2T_x$ MXene accumulates a negative charge, while TiO_2 becomes positively charged, leading to the formation of a Schottky barrier at the $Ti_3C_2T_x$–TiO_2 interface, serving as a space-charge layer. Subsequently, the photogenerated electrons on $Ti_3C_2T_x$ MXene migrate to its surface, where they react with O_2 molecules to generate superoxide radicals ($\bullet O^{2-}$) [115,145]. Meanwhile, the photogenerated holes react with adsorbed hydroxyl ions (OH^-) to form hydroxyl radicals ($\bullet OH$) [54]. These radicals play a crucial role in the degradation of MO. The photocatalytic reaction mechanism as facilitated by the MXene-based hybrid photocatalyst ($TiO_2/Ti_3C_2T_x$) is illustrated in **Figure 4**a [115]. The mechanism can be roughly described through the following reactions:

$$Ti_3C_2–TiO_2 + h\upsilon \rightarrow TiO_2\ (h+) + Ti_3C_2\ (e^-) \quad (1)$$

$$h^+ + OH– \rightarrow \bullet OH \quad (2)$$

$$e^- + O2 \rightarrow \bullet O^{2-} \quad (3)$$

$$\text{Dye (Anionic or cationic)} + \bullet O^{2-} \rightarrow \quad CO_2 + H_2O \quad (4)$$

$$\text{Dye (Anionic or cationic)} + \bullet OH \rightarrow \quad CO_2 + H_2O \quad (5)$$

 doi:10.20944/preprints202502.1240.v1

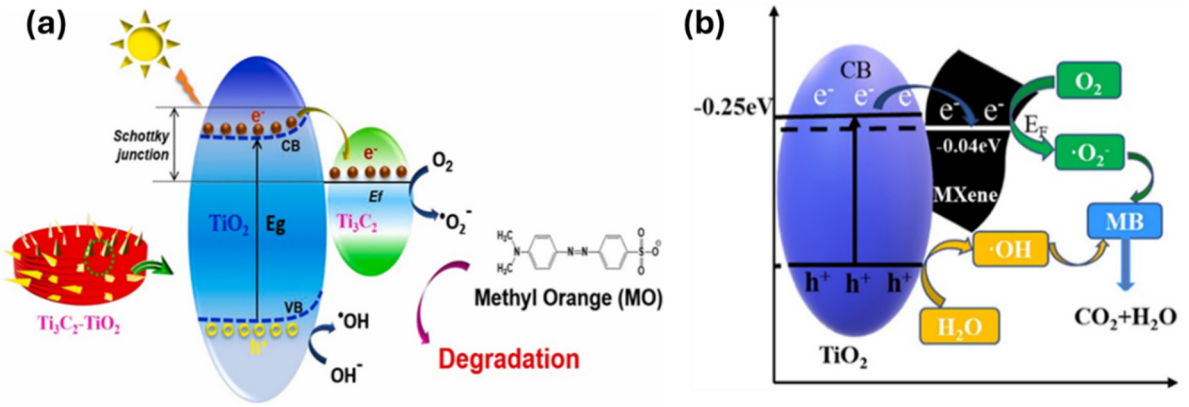

Figure 4. Proposed mechanism of (a) anionic dye, MO, (Adapted from Ref [115]) and (b) cationic dye, MB, photocatalysis over the $TiO_2/Ti_3C_2T_x$ composite (Adapted from Ref [146]).

For the degradation of a cationic dye like Methylene Blue (MB), superoxide radical anions ($•O^{2-}$) are produced through a reduction reaction between electrons and O_2 molecules, leading to the direct degradation of MB. Additionally, the light-induced h^+ partially oxidizes MB and partially reacts with water to generate hydroxyl radicals, ultimately breaking down MB.[147]. It is evident from **Figure 4**b that •OH and h^+ are the primary reactive species in the $TiO_2/Ti_3C_2T_x$ MXene composite photocatalysis reaction system [146]. Ultimately, the radicals (•OH, $•O^{2-}$) possessing strong oxidizing abilities, degrade both anionic and cationic dyes, such as MO and MB molecules, directly into their oxidation products[148,149]. Therefore, a similar photocatalytic reaction mechanism occurs for both cationic and anionic dyes under light irradiation.

8. Challenges and Future Directions

$Ti_3C_2T_x$ MXene-based hybrid photocatalysts have emerged as promising materials for the degradation of organic dye pollutants, demonstrating significant potential in environmental remediation. However, despite their advantages for applications in organic dye degradation, several challenges remain that must be addressed to further enhance their photocatalytic performance and facilitate their practical application.

While $Ti_3C_2T_x$ MXene-based photocatalysts exhibit impressive photocatalytic activity towards dye degradation, the development of green synthesis methods is one of the biggest challenges in MXene research. Most of the current synthesis processes involves harsh and hazardous chemicals for etching and exfoliation such as hydrofluoric acid and tetramethylammonium hydroxide and tetrabutylammonium hydroxide [35]. The elimination of such chemicals from the synthesis process is highly desirable for the wide applicability of MXenes. Furthermore, the limited yield of the final MXene product during synthesis is another limiting factor. As of this date, the large-scale synthesis processes for high-quality MXenes are known to be inefficient. Hence the development of mass-production methods for high-quality and uniformly delaminated single to few-layer MXenes nanosheets is required for commercial use. Future research efforts should focus on the reaction kinetics and thermodynamics of the synthesis process for uniform and mass production of MXenes.

The long-term stability of MXenes in harsh environmental conditions such as oxygen, high humidity, and acidic or alkaline media is another concern [37].The corrosion and degradation of MXenes over time can compromise the catalytic efficiency of the composite materials and hinder their reuse. The thermal stability is also considerable challenge for MXene-based photocatalysts as the increased temperature can boost the MXene oxidation [150].

Over the years, significant efforts have been put together to address the challenges associated with MXenes-based hybrid photocatalysts. Future research efforts should focus on the reaction kinetics and thermodynamics of the synthesis process for uniform and mass production of MXene photocatalyst. Considering future developments and practical applications, the large-scale synthesis

 doi:10.20944/preprints202502.1240.v1

routes without the use of environmentally hazardous chemicals and the antioxidation strategies of MXenes should be explored.

For $Ti_3C_2T_x$ MXene-based hybrid photocatalysts to transition from the laboratory to real-world applications, strategies to integrate them into practical systems, such as water treatment plants or portable water purification devices, should be explored. The development of easy-to-apply photocatalytic reactors or devices that utilize MXene-based hybrid materials for the degradation of organic dyes and other pollutants will help bring these materials to the forefront of environmental remediation technologies. To enhance the efficiency of $Ti_3C_2T_x$ MXene-based hybrid photocatalysts, a predictive design approach leveraging modern AI and existing databases can be utilized to identify and screen suitable materials for improved performance.

9. Conclusion

In conclusion, we reviewed fabrication of $Ti_3C_2T_x$ MXene-based hybrid photocatalysts and evaluated them for their role in the degradation of cationic and anionic organic dyes. $Ti_3C_2T_x$ MXene has been found to exhibit exceptional physical and chemical properties, including high electrical conductivity, excellent hydrophilicity, adsorption capability, and efficient charge transfer, while also suppressing electron-hole recombination in the photocatalyst material during photocatalysis. $Ti_3C_2T_x$ MXene has emerged as a promising alternative to noble metal catalysts, providing low-cost, scalable synthesis options along with exceptional catalytic performance for hybrid photocatalysts. Our evaluation demonstrated that $Ti_3C_2T_x$ MXene-based hybrid photocatalysts significantly enhanced dye degradation efficiency, as reflected in both the percentage degradation and reduced degradation time, compared to nonhybrid or pure semiconducting materials. A comprehensive understanding of the dye degradation mechanisms involving $Ti_3C_2T_x$ MXene-based hybrid photocatalysts has also been provided. Additionally, various computational studies and simulations have been conducted to advance research efforts in dye degradation using these photocatalysts. Lastly, the challenges associated with $Ti_3C_2T_x$ MXene-based hybrid photocatalysts have been thoroughly identified, and future research directions have been suggested to address these challenges effectively.

Acknowledgments: T. L. sincerely acknowledges support for this project provided by the Faculty Research Support Fund (FRSF), UHCL (Award # $2408). F.Y. acknowledges support from the U.S. National Science Foundation (NSF) under grant #DMR-2122044 and the U.S. Army Research Office (ARO) under grant # W911NF2210109. J.P. acknowledges support from the endowed professorship in science # 45 for 2024-2025 from McNeese State University.

References

1. Singh, B.J.; Chakraborty, A.; Sehgal, R. A Systematic Review of Industrial Wastewater Management: Evaluating Challenges and Enablers. *J. Environ. Manage.* **2023**, *348*, 119230, doi:10.1016/j.jenvman.2023.119230.
2. Ahmed, J.; Thakur, A.; Goyal, A. Industrial Wastewater and Its Toxic Effects. In *Biological Treatment of Industrial Wastewater*; Shah, M.P., Ed.; The Royal Society of Chemistry, 2021; pp. 1–14 ISBN 978-1-83916-279-4.
3. López-Ahumada, E.; Salazar-Hernández, M.; Talavera-López, A.; Solis-Marcial, O.J.; Hernández-Soto, R.; Ruelas-Leyva, J.P.; Hernández, J.A. Removal of Anionic and Cationic Dyes Present in Solution Using Biomass of Eichhornia Crassipes as Bioadsorbent. *Molecules* **2022**, *27*, 6442, doi:10.3390/molecules27196442.
4. Salleh, M.A.M.; Mahmoud, D.K.; Karim, W.A.W.A.; Idris, A. Cationic and Anionic Dye Adsorption by Agricultural Solid Wastes: A Comprehensive Review. *Desalination* **2011**, *280*, 1–13, doi:10.1016/j.desal.2011.07.019.
5. Zhong, Q.; Li, Y.; Zhang, G. Two-Dimensional MXene-Based and MXene-Derived Photocatalysts: Recent Developments and Perspectives. *Chem. Eng. J.* **2021**, *409*, 128099, doi:10.1016/j.cej.2020.128099.
6. Nasri, M.S.I.; Samsudin, M.F.R.; Tahir, A.A.; Sufian, S. Effect of MXene Loaded on G-C_3N_4 Photocatalyst for the Photocatalytic Degradation of Methylene Blue. *Energies* **2022**, *15*, 955, doi:10.3390/en15030955.

7. Lee, Q.Y.; Li, H. Photocatalytic Degradation of Plastic Waste: A Mini Review *Micromachines* **2021**, *12*, 907, doi:10.3390/mi12080907.
8. Khan, S.; Noor, T.; Iqbal, N.; Yaqoob, L. Photocatalytic Dye Degradation from Textile Wastewater: A Review. *ACS Omega* **2024**, *9*, 21751–21767, doi:10.1021/acsomega.4c00887.
9. Gupta, T.; Chauhan, R.P. Photocatalytic Degradation of Water Pollutants Using II-VI Semiconducting Catalysts: A Comprehensive Review. *J. Environ. Chem. Eng.* **2021**, *9*, 106734, doi:10.1016/j.jece.2021.106734.
10. Rafiq, A.; Ikram, M.; Ali, S.; Niaz, F.; Khan, M.; Khan, Q.; Maqbool, M. Photocatalytic Degradation of Dyes Using Semiconductor Photocatalysts to Clean Industrial Water Pollution. *J. Ind. Eng. Chem.* **2021**, *97*, 111–128, doi:10.1016/j.jiec.2021.02.017.
11. Guo, R.; Wang, J.; Bi, Z.; Chen, X.; Hu, X.; Pan, W. Recent Advances and Perspectives of g–C_3N_4–Based Materials for Photocatalytic Dyes Degradation. *Chemosphere* **2022**, *295*, 133834, doi:10.1016/j.chemosphere.2022.133834.
12. Yadav, S.; Shakya, K.; Gupta, A.; Singh, D.; Chandran, A.R.; Varayil Aanappalli, A.; Goyal, K.; Rani, N.; Saini, K. A Review on Degradation of Organic Dyes by Using Metal Oxide Semiconductors. *Environ. Sci. Pollut. Res.* **2022**, *30*, 71912–71932, doi:10.1007/s11356-022-20818-6.
13. Wu, L.; Li, Q.; Yang, C.; Ma, X.; Zhang, Z.; Cui, X. Constructing a Novel TiO_2 /γ-Graphyne Heterojunction for Enhanced Photocatalytic Hydrogen Evolution. *J. Mater. Chem. A* **2018**, *6*, 20947–20955, doi:10.1039/C8TA07307D.
14. Li, X.; Yu, J.; Wageh, S.; Al-Ghamdi, A.A.; Xie, J. Graphene in Photocatalysis: A Review. *Small* **2016**, *12*, 6640–6696, doi:10.1002/smll.201600382.
15. Yang, J.; Wang, D.; Han, H.; Li, C. Roles of Cocatalysts in Photocatalysis and Photoelectrocatalysis. *Acc. Chem. Res.* **2013**, *46*, 1900–1909, doi:10.1021/ar300227e.
16. Ramalingam, G.; Perumal, N.; Priya, A.K.; Rajendran, S. A Review of Graphene-Based Semiconductors for Photocatalytic Degradation of Pollutants in Wastewater. *Chemosphere* **2022**, *300*, 134391, doi:10.1016/j.chemosphere.2022.134391.
17. Zhou, W.; Pan, K.; Qu, Y.; Sun, F.; Tian, C.; Ren, Z.; Tian, G.; Fu, H. Photodegradation of Organic Contamination in Wastewaters by Bonding TiO_2/Single-Walled Carbon Nanotube Composites with Enhanced Photocatalytic Activity. *Chemosphere* **2010**, *81*, 555–561, doi:10.1016/j.chemosphere.2010.08.059.
18. Sharma, S.; Dutta, V.; Singh, P.; Raizada, P.; Rahmani-Sani, A.; Hosseini-Bandegharaei, A.; Thakur, V.K. Carbon Quantum Dot Supported Semiconductor Photocatalysts for Efficient Degradation of Organic Pollutants in Water: A Review. *J. Clean. Prod.* **2019**, *228*, 755–769, doi:10.1016/j.jclepro.2019.04.292.
19. Tong, T.; Zhang, M.; Chen, W.; Huo, X.; Xu, F.; Yan, H.; Lai, C.; Wang, W.; Hu, S.; Qin, L.; et al. Recent Advances in Carbon-Based Material/Semiconductor Composite Photoelectrocatalysts: Synthesis, Improvement Strategy, and Organic Pollutant Removal. *Coord. Chem. Rev.* **2024**, *500*, 215498, doi:10.1016/j.ccr.2023.215498.
20. Li, X.; Bai, Y.; Shi, X.; Su, N.; Nie, G.; Zhang, R.; Nie, H.; Ye, L. Applications of MXene ($Ti_3C_2T_x$) in Photocatalysis: A Review. *Mater. Adv.* **2021**, *2*, 1570–1594, doi:10.1039/D0MA00938E.
21. Im, J.K.; Sohn, E.J.; Kim, S.; Jang, M.; Son, A.; Zoh, K.-D.; Yoon, Y. Review of MXene-Based Nanocomposites for Photocatalysis. *Chemosphere* **2021**, *270*, 129478, doi:10.1016/j.chemosphere.2020.129478.
22. Murali, G.; Reddy Modigunta, J.K.; Park, Y.H.; Lee, J.-H.; Rawal, J.; Lee, S.-Y.; In, I.; Park, S.-J. A Review on MXene Synthesis, Stability, and Photocatalytic Applications. *ACS Nano* **2022**, *16*, 13370–13429, doi:10.1021/acsnano.2c04750.
23. Ning, X.; Hao, A.; Cao, Y.; Chen, R.; Xie, J.; Lu, Z.; Hu, J.; Jia, D. Construction of MXene/Bi_2WO_6 Schottky Junction for Highly Efficient Piezocatalytic Hydrogen Evolution and Unraveling Mechanism. *Nano Lett.* **2024**, *24*, 3361–3368, doi:10.1021/acs.nanolett.3c04959.
24. Sinopoli, A.; Othman, Z.; Rasool, K.; Mahmoud, K.A. Electrocatalytic/Photocatalytic Properties and Aqueous Media Applications of 2D Transition Metal Carbides (MXenes). *Curr. Opin. Solid State Mater. Sci.* **2019**, *23*, 100760, doi:10.1016/j.cossms.2019.06.004.
25. Cui, L.; Wen, J.; Deng, Q.; Du, X.; Tang, T.; Li, M.; Xiao, J.; Jiang, L.; Hu, G.; Cao, X.; et al. Improving the Photocatalytic Activity of Ti_3C_2 MXene by Surface Modification of N Doped. *Materials* **2023**, *16*, 2836, doi:10.3390/ma16072836.

26. Huang, K.; Li, C.; Li, H.; Ren, G.; Wang, L.; Wang, W.; Meng, X. Photocatalytic Applications of Two-Dimensional Ti_3C_2 MXenes: A Review. *ACS Appl. Nano Mater.* **2020**, *3*, 9581–9603, doi:10.1021/acsanm.0c02481.
27. Tang, R.; Xiong, S.; Gong, D.; Deng, Y.; Wang, Y.; Su, L.; Ding, C.; Yang, L.; Liao, C. Ti_3C_2 2D MXene: Recent Progress and Perspectives in Photocatalysis. *ACS Appl. Mater. Interfaces* **2020**, *12*, 56663–56680, doi:10.1021/acsami.0c12905.
28. Illahi, C.; Hutabarat, W.E.F.; Nurdini, N.; Failamani, F.; Kadja, G.T.M. Photocatalytic Degradation of Azo Dyes over MXene-Based Catalyst: Recent Developments and Future Prospects. *Nanotechnol.* **2024**, *6*, 100055, doi:10.1016/j.nxnano.2024.100055.
29. Li, X.; Bai, Y.; Shi, X.; Su, N.; Nie, G.; Zhang, R.; Nie, H.; Ye, L. Applications of MXene ($Ti_3C_2T_x$) in Photocatalysis: A Review. *Mater. Adv.* **2021**, *2*, 1570–1594, doi:10.1039/D0MA00938E.
30. Goel, N.; Kushwaha, A.; Kumar, M. Two-Dimensional MXenes: Recent Emerging Applications. *RSC Adv.* **2022**, *12*, 25172–25193, doi:10.1039/D2RA04354H.
31. Kitchamsetti, N.; De Barros, A.L.F. Recent Advances in MXenes Based Composites as Photocatalysts: Synthesis, Properties and Photocatalytic Removal of Organic Contaminants from Wastewater. *ChemCatChem* **2023**, *15*, e202300690, doi:10.1002/cctc.202300690.
32. Peng, C.; Zhou, T.; Wei, P.; Xu, W.; Pan, H.; Peng, F.; Jia, J.; Zhang, K.; Yu, H. Photocatalysis over MXene-Based Hybrids: Synthesis, Surface Chemistry, and Interfacial Charge Kinetics. *APL Mater.* **2021**, *9*, 070703, doi:10.1063/5.0055711.
33. Javaid, A.; Latif, S.; Imran, M.; Hussain, N.; Bilal, M.; Iqbal, H.M.N. MXene-Based Hybrid Composites as Photocatalyst for the Mitigation of Pharmaceuticals. *Chemosphere* **2022**, *291*, 133062, doi:10.1016/j.chemosphere.2021.133062.
34. Iravani, S.; Varma, R.S. MXene-Based Photocatalysts in Degradation of Organic and Pharmaceutical Pollutants. *Molecules* **2022**, *27*, 6939, doi:10.3390/molecules27206939.
35. Naguib, M.; Kurtoglu, M.; Presser, V.; Lu, J.; Niu, J.; Heon, M.; Hultman, L.; Gogotsi, Y.; Barsoum, M.W. Two-Dimensional Nanocrystals Produced by Exfoliation of Ti_3AlC_2. *Adv. Mater.* **2011**, *23*, 4248–4253, doi:10.1002/adma.201102306.
36. Ayad, M.M.; El-Nasr, A.A. Anionic Dye (Acid Green 25) Adsorption from Water by Using Polyaniline Nanotubes Salt/Silica Composite. *J. Nanostructure Chem.* **2012**, *3*, 3, doi:10.1186/2193-8865-3-3.
37. Limbu, T.B.; Chitara, B.; Orlando, J.D.; Garcia Cervantes, M.Y.; Kumari, S.; Li, Q.; Tang, Y.; Yan, F. Green Synthesis of Reduced $Ti_3C_2T_x$ MXene Nanosheets with Enhanced Conductivity, Oxidation Stability, and SERS Activity. *J. Mater. Chem. C* **2020**, *8*, 4722–4731, doi:10.1039/C9TC06984D.
38. Wang, D.; Zhou, C.; Filatov, A.S.; Cho, W.; Lagunas, F.; Wang, M.; Vaikuntanathan, S.; Liu, C.; Klie, R.F.; Talapin, D.V. Direct Synthesis and Chemical Vapor Deposition of 2D Carbide and Nitride MXenes. *Science* **2023**, *379*, 1242–1247, doi:10.1126/science.add9204.
39. Ayodhya, D. A Review of Recent Progress in 2D MXenes: Synthesis, Properties, and Applications. *Diam. Relat. Mater.* **2023**, *132*, 109634, doi:10.1016/j.diamond.2022.109634.
40. Lei, J.-C.; Zhang, X.; Zhou, Z. Recent Advances in MXene: Preparation, Properties, and Applications. *Front. Phys.* **2015**, *10*, 276–286, doi:10.1007/s11467-015-0493-x.
41. Xu, X.; Zhang, C.; Yin, J.; Smajic, J.; Bahabri, M.; Lei, Y.; Hedhili, M.N.; Hota, M.K.; Shi, L.; Guo, T.; et al. Anisotropic Superconducting Nb_2CT_x MXene Processed by Atomic Exchange at the Wafer Scale. *Adv. Mater.* **2024**, *36*, 2305326, doi:10.1002/adma.202305326.
42. Kamysbayev, V.; Filatov, A.S.; Hu, H.; Rui, X.; Lagunas, F.; Wang, D.; Klie, R.F.; Talapin, D.V. Covalent Surface Modifications and Superconductivity of Two-Dimensional Metal Carbide MXenes. *Science* **2020**, *369*, 979–983, doi:10.1126/science.aba8311.
43. Gogotsi, Y.; Anasori, B. The Rise of MXenes. *ACS Nano* **2019**, *13*, 8491–8494, doi:10.1021/acsnano.9b06394.
44. Verger, L.; Xu, C.; Natu, V.; Cheng, H.-M.; Ren, W.; Barsoum, M.W. Overview of the Synthesis of MXenes and Other Ultrathin 2D Transition Metal Carbides and Nitrides. *Curr. Opin. Solid State Mater. Sci.* **2019**, *23*, 149–163, doi:10.1016/j.cossms.2019.02.001.
45. Liu, H.; Guo, H.; Gao, Z.; Pan, H.; Zhen, J.; Linghu, J.; Li, Z. Applications of Artificial Intelligence in Materials Research for Fuel Cells. *AI Mater.* **2025**, doi:10.55092/aimat20250003.

46. Alhabeb, M.; Maleski, K.; Anasori, B.; Lelyukh, P.; Clark, L.; Sin, S.; Gogotsi, Y. Guidelines for Synthesis and Processing of Two-Dimensional Titanium Carbide ($Ti_3C_2T_x$ MXene). *Chem. Mater.* **2017**, *29*, 7633–7644, doi:10.1021/acs.chemmater.7b02847.
47. Koh, S.W.; Rekhi, L.; Arramel; Birowosuto, M.D.; Trinh, Q.T.; Ge, J.; Yu, W.; Wee, A.T.S.; Choksi, T.S.; Li, H. Tuning the Work Function of MXene via Surface Functionalization. *ACS Appl. Mater. Interfaces* **2024**, *16*, 66826–66836, doi:10.1021/acsami.3c11857.
48. Guo, L.; Jiang, W.-Y.; Shen, M.; Xu, C.; Ding, C.-X.; Zhao, S.-F.; Yuan, T.-T.; Wang, C.-Y.; Zhang, X.-Q.; Wang, J.-Q. High Capacitance of MXene (Ti_3C_2T) through Intercalation and Surface Modification in Molten Salt. *Electrochimica Acta* **2022**, *401*, 139476, doi:10.1016/j.electacta.2021.139476.
49. Cao, Z.; Yin, Q.; Zhang, Y.; Li, Y.; Yu, C.; Zhang, M.; Fan, B.; Shao, G.; Wang, H.; Xu, H.; et al. Heterostructure Composites of TiO_2 and CdZnS Nanoparticles Decorated on $Ti_3C_2T_x$ Nanosheets and Their Enhanced Photocatalytic Performance by Microwave Hydrothermal Method. *J. Alloys Compd.* **2022**, *918*, 165681, doi:10.1016/j.jallcom.2022.165681.
50. Purbayanto, M.A.K.; Bury, D.; Chandel, M.; Shahrak, Z.D.; Mochalin, V.N.; Wójcik, A.; Moszczyńska, D.; Wojciechowska, A.; Tabassum, A.; Naguib, M.; et al. Ambient Processed rGO/Ti_3CNT_x MXene Thin Film with High Oxidation Stability, Photosensitivity, and Self-Cleaning Potential. *ACS Appl. Mater. Interfaces* **2023**, *15*, 44075–44086, doi:10.1021/acsami.3c07972.
51. Cao, S.; Shen, B.; Tong, T.; Fu, J.; Yu, J. 2D/2D Heterojunction of Ultrathin MXene/Bi_2WO_6 Nanosheets for Improved Photocatalytic CO_2 Reduction. *Adv. Funct. Mater.* **2018**, *28*, 1800136, doi:10.1002/adfm.201800136.
52. Latif, F.E.A.; Khalid, M.; Numan, A.; Manaf, N.A.; Mubarak, N.M.; Zaharin, H.A.; Abdullah, E.C. Microwave-Assisted Hydrothermal Synthesis of $Ti_3C_2T_x$ MXene: A Sustainable and Scalable Approach Using Alkaline Etchant. *J. Mol. Struct.* **2025**, *1329*, 141407, doi:10.1016/j.molstruc.2025.141407.
53. My Tran, N.; Thanh Hoai Ta, Q.; Noh, J.-S. Unusual Synthesis of Safflower-Shaped TiO_2/Ti_3C_2 Heterostructures Initiated from Two-Dimensional Ti_3C_2 MXene. *Appl. Surf. Sci.* **2021**, *538*, 148023, doi:10.1016/j.apsusc.2020.148023.
54. Quyen, V.T.; Ha, L.T.T.; Thanh, D.M.; Le, Q.V.; Viet, N.M.; Nham, N.T.; Thang, P.Q. Advanced Synthesis of MXene-Derived Nanoflower-Shaped TiO_2@Ti 3 C 2 Heterojunction to Enhance Photocatalytic Degradation of Rhodamine B. *Environ. Technol. Innov.* **2021**, *21*, 101286, doi:10.1016/j.eti.2020.101286.
55. Chen, J.; Zheng, H.; Zhao, Y.; Que, M.; Lei, X.; Zhang, K.; Luo, Y. Preparation of Facet Exposed TiO_2/Ti_3C_2T Composites with Enhanced Photocatalytic Activity. *J. Phys. Chem. Solids* **2020**, *145*, 109565, doi:10.1016/j.jpcs.2020.109565.
56. Ta, Q.T.H.; Tran, N.M.; Noh, J.-S. Rice Crust-Like ZnO/$Ti_3C_2T_x$ MXene Hybrid Structures for Improved Photocatalytic Activity. *Catalysts* **2020**, *10*, 1140, doi:10.3390/catal10101140.
57. Nasri, M.S.I.; Samsudin, M.F.R.; Tahir, A.A.; Sufian, S. Effect of MXene Loaded on G-C_3N_4 Photocatalyst for the Photocatalytic Degradation of Methylene Blue. *Energies* **2022**, *15*, 955, doi:10.3390/en15030955.
58. Cai, T.; Wang, L.; Liu, Y.; Zhang, S.; Dong, W.; Chen, H.; Yi, X.; Yuan, J.; Xia, X.; Liu, C.; et al. Ag_3PO_4/Ti_3C_2 MXene Interface Materials as a Schottky Catalyst with Enhanced Photocatalytic Activities and Anti-Photocorrosion Performance. *Appl. Catal. B Environ.* **2018**, *239*, 545–554, doi:10.1016/j.apcatb.2018.08.053.
59. Fan, Y.; Liu, Z.; Li, Q.; Zhao, K.; Ahmad, M.; Liu, P.; Zhang, Q.; Zhang, B. Preparation of MoS_2 /MXene/NC Porous Composite Microspheres with Wrinkled Surface and Their Microwave Absorption Performances. *ACS Appl. Mater. Interfaces* **2023**, *15*, 41720–41731, doi:10.1021/acsami.3c08563.
60. Jin Lee, D.; Mohan Kumar, G.; Sekar, S.; Chang Jeon, H.; Young Kim, D.; Ilanchezhiyan, P. Ultrasonic Processing of WO_3 Nanosheets Integrated Ti_3C_2 MXene 2D-2D Based Heterojunctions with Synergistic Effects for Enhanced Water Splitting and Environmental Remediation. *Ultrason. Sonochem.* **2023**, *101*, 106681, doi:10.1016/j.ultsonch.2023.106681.
61. Alsafari, I.A.; Munir, S.; Zulfiqar, S.; Saif, M.S.; Warsi, M.F.; Shahid, M. Synthesis, Characterization, Photocatalytic and Antibacterial Properties of Copper Ferrite/MXene ($CuFe_2O_4/Ti_3C_2$) Nanohybrids. *Ceram. Int.* **2021**, *47*, 28874–28883, doi:10.1016/j.ceramint.2021.07.048.

 doi:10.20944/preprints202502.1240.v1

62. Liu, X.; Liu, Q.; Chen, C. Ultrasonic Oscillation Synthesized ZnS Nanoparticles/Layered MXene Sheet with Outstanding Photocatalytic Activity under Visible Light. *Vacuum* **2021**, *183*, 109834, doi:10.1016/j.vacuum.2020.109834.
63. Ishfaq, M.; Rasheed, A.; Ajmal, S.; Dastgeer, G.; Naz, T.; Baig, M.M.; Lee, S.G. Synthesis and Characterization of a Novel MnO_2@MXene-Based 2D/3D Hierarchical Z-Scheme for Sustainable Environmental Applications. *Ceram. Int.* **2024**, *50*, 9801–9810, doi:10.1016/j.ceramint.2023.12.301.
64. Iqbal, M.A.; Tariq, A.; Zaheer, A.; Gul, S.; Ali, S.I.; Iqbal, M.Z.; Akinwande, D.; Rizwan, S. Ti_3C_2 -MXene/Bismuth Ferrite Nanohybrids for Efficient Degradation of Organic Dyes and Colorless Pollutants. *ACS Omega* **2019**, *4*, 20530–20539, doi:10.1021/acsomega.9b02359.
65. Iqbal, M.A.; Ali, S.I.; Amin, F.; Tariq, A.; Iqbal, M.Z.; Rizwan, S. La- and Mn-Codoped Bismuth Ferrite/Ti_3C_2 MXene Composites for Efficient Photocatalytic Degradation of Congo Red Dye. *ACS Omega* **2019**, *4*, 8661–8668, doi:10.1021/acsomega.9b00493.
66. Zheng, W.; Zhang, P.; Tian, W.; Wang, Y.; Zhang, Y.; Chen, J.; Sun, Z. Microwave-Assisted Synthesis of SnO2-Ti_3C_2 Nanocomposite for Enhanced Supercapacitive Performance. *Mater. Lett.* **2017**, *209*, 122–125, doi:10.1016/j.matlet.2017.07.131.
67. Zhou, W.; Zhu, J.; Wang, F.; Cao, M.; Zhao, T. One-Step Synthesis of Ceria/Ti_3C_2 Nanocomposites with Enhanced Photocatalytic Activity. *Mater. Lett.* **2017**, *206*, 237–240, doi:10.1016/j.matlet.2017.06.117.
68. Sajid, M.M.; Khan, S.B.; Javed, Y.; Amin, N.; Zhang, Z.; Shad, N.A.; Zhai, H. Bismuth Vanadate/MXene ($BiVO_4$ /Ti_3C_2) Heterojunction Composite: Enhanced Interfacial Control Charge Transfer for Highly Efficient Visible Light Photocatalytic Activity. *Environ. Sci. Pollut. Res.* **2021**, *28*, 35911–35923, doi:10.1007/s11356-021-13315-9.
69. Jiao, S.; Liu, L. Friction-Induced Enhancements for Photocatalytic Degradation of MoS_2 @Ti_3C_2 Nanohybrid. *Ind. Eng. Chem. Res.* **2019**, *58*, 18141–18148, doi:10.1021/acs.iecr.9b03680.
70. Zhang, S.; Cai, M.; Wu, J.; Wang, Z.; Lu, X.; Li, K.; Lee, J.-M.; Min, Y. Photocatalytic Degradation of TiO_2 via Incorporating Ti_3C_2 MXene for Methylene Blue Removal from Water. *Catal. Commun.* **2023**, *174*, 106594, doi:10.1016/j.catcom.2022.106594.
71. Othman, Z.; Sinopoli, A.; Mackey, H.R.; Mahmoud, K.A. Efficient Photocatalytic Degradation of Organic Dyes by $AgNPs$/TiO_2 /$Ti_3C_2T_x$ MXene Composites under UV and Solar Light. *ACS Omega* **2021**, *6*, 33325–33338, doi:10.1021/acsomega.1c03189.
72. Ighalo, J.O.; Smith, M.L.; Mayyahi, A.A.; Amama, P.B. MXenes in Photocatalytic NOx Abatement: Current Innovations, Opportunities, and Challenges. *Appl. Catal. B Environ. Energy* **2024**, *358*, 124352, doi:10.1016/j.apcatb.2024.124352.
73. Lei, J.-C.; Zhang, X.; Zhou, Z. Recent Advances in MXene: Preparation, Properties, and Applications. *Front. Phys.* **2015**, *10*, 276–286, doi:10.1007/s11467-015-0493-x.
74. Ahmaruzzaman, Md. MXenes and MXene-Supported Nanocomposites: A Novel Materials for Aqueous Environmental Remediation. *RSC Adv.* **2022**, *12*, 34766–34789, doi:10.1039/D2RA05530A.
75. Ahmaruzzaman, Md. MXene-Based Novel Nanomaterials for Remediation of Aqueous Environmental Pollutants. *Inorg. Chem. Commun.* **2022**, *143*, 109705, doi:10.1016/j.inoche.2022.109705.
76. Atri, S.; Loni, E.; Zazimal, F.; Hensel, K.; Caplovicova, M.; Plesch, G.; Lu, X.; Nagarajan, R.; Naguib, M.; Monfort, O. MXene-Derived Oxide Nanoheterostructures for Photocatalytic Sulfamethoxazole Degradation. *ACS Appl. Nano Mater.* **2024**, *7*, 16506–16515, doi:10.1021/acsanm.4c02523.
77. Kumar, A.; Dixit, U.; Singh, K.; Prakash Gupta, S.; S. Jamal Beg, M. Structure and Properties of Dyes and Pigments. In *Dyes and Pigments - Novel Applications and Waste Treatment*; Papadakis, R., Ed.; IntechOpen, 2021 ISBN 978-1-83968-614-6.
78. Javaid, A.; Latif, S.; Imran, M.; Hussain, N.; Bilal, M.; Iqbal, H.M.N. MXene-Based Hybrid Composites as Photocatalyst for the Mitigation of Pharmaceuticals. *Chemosphere* **2022**, *291*, 133062, doi:10.1016/j.chemosphere.2021.133062.
79. Wang, C.; Ye, J.; Liang, L.; Cui, X.; Kong, L.; Li, N.; Cheng, Z.; Peng, W.; Yan, B.; Chen, G. Application of MXene-Based Materials in Fenton-like Systems for Organic Wastewater Treatment: A Review. *Sci. Total Environ.* **2023**, *862*, 160539, doi:10.1016/j.scitotenv.2022.160539.

80. Amrillah, T.; Supandi, A.R.; Puspasari, V.; Hermawan, A.; Seh, Z.W. MXene-Based Photocatalysts and Electrocatalysts for CO_2 Conversion to Chemicals. *Trans. Tianjin Univ.* **2022**, *28*, 307–322, doi:10.1007/s12209-022-00328-9.
81. Dey, P.Ch.; Das, R. Enhanced Photocatalytic Degradation of Methyl Orange Dye on Interaction with Synthesized Ligand Free CdS Nanocrystals under Visible Light Illumination. *Spectrochim. Acta. A. Mol. Biomol. Spectrosc.* **2020**, *231*, 118122, doi:10.1016/j.saa.2020.118122.
82. Medina, J.C.; Bizarro, M.; Silva-Bermudez, P.; Giorcelli, M.; Tagliaferro, A.; Rodil, S.E. Photocatalytic Discoloration of Methyl Orange Dye by δ-Bi2O3 Thin Films. *Thin Solid Films* **2016**, *612*, 72–81, doi:10.1016/j.tsf.2016.05.034.
83. Al-Tohamy, R.; Ali, S.S.; Li, F.; Okasha, K.M.; Mahmoud, Y.A.-G.; Elsamahy, T.; Jiao, H.; Fu, Y.; Sun, J. A Critical Review on the Treatment of Dye-Containing Wastewater: Ecotoxicological and Health Concerns of Textile Dyes and Possible Remediation Approaches for Environmental Safety. *Ecotoxicol. Environ. Saf.* **2022**, *231*, 113160, doi:10.1016/j.ecoenv.2021.113160.
84. Srisai, J.; Muangnapoh, T.; Vas-Umnuay, P. Comparative Study on Photocatalytic Degradation of Methylene Blue Using Pristine ZnO and Ni/ZnO Composite Films. *Mater. Today Proc.* **2022**, *66*, 3168–3173, doi:10.1016/j.matpr.2022.06.398.
85. Mohammad Jafri, N.; Jaafar, J.; Alias, N.; Samitsu, S.; Aziz, F.; Wan Salleh, W.; Mohd Yusop, M.; Othman, M.; Rahman, M.; Ismail, A.; et al. Synthesis and Characterization of Titanium Dioxide Hollow Nanofiber for Photocatalytic Degradation of Methylene Blue Dye. *Membranes* **2021**, *11*, 581, doi:10.3390/membranes11080581.
86. Seling, T.R.; Katzbaer, R.R.; Thompson, K.L.; Aksoy, S.E.; Chitara, B.; Shringi, A.K.; Schaak, R.E.; Riaz, U.; Yan, F. Transition Metal-Doped CuO Nanosheets for Enhanced Visible-Light Photocatalysis. *J. Photochem. Photobiol. Chem.* **2024**, *448*, 115356, doi:10.1016/j.jphotochem.2023.115356.
87. Seling, T.R.; Kumar Shringi, A.; Wang, K.; Riaz, U.; Yan, F. Bi2O2S Nanosheets for Effective Visible Light Photocatalysis of Anionic Dye Degradation. *Mater. Lett.* **2024**, *361*, 136136, doi:10.1016/j.matlet.2024.136136.
88. Mary A, S.; Norbert, A.; Shaji, S.; Philip, R.R. Electrochemically Anodized Solid and Stable ZnO Nanorods as an Adsorbent/ Nanophotocatalyst: ROS Mediated Degradation of Azo Dyes Congo Red and Methyl Orange. *J. Clean. Prod.* **2023**, *428*, 139466, doi:10.1016/j.jclepro.2023.139466.
89. Mittal, H.; Khanuja, M. Optimization of MoSe2 Nanostructure by Surface Modification Using Conducting Polymer for Degradation of Cationic and Anionic Dye: Photocatalysis Mechanism, Reaction Kinetics and Intermediate Product Study. *Dyes Pigments* **2020**, *175*, 108109, doi:10.1016/j.dyepig.2019.108109.
90. Fang, S.; Lv, K.; Li, Q.; Ye, H.; Du, D.; Li, M. Effect of Acid on the Photocatalytic Degradation of Rhodamine B over G-C_3N_4. *Appl. Surf. Sci.* **2015**, *358*, 336–342, doi:10.1016/j.apsusc.2015.07.179.
91. Revathi, B.; Balakrishnan, L.; Pichaimuthu, S.; Nirmala Grace, A.; Krishna Chandar, N. Photocatalytic Degradation of Rhodamine B Using BiMnO3 Nanoparticles under UV and Visible Light Irradiation. *J. Mater. Sci. Mater. Electron.* **2020**, *31*, 22487–22497, doi:10.1007/s10854-020-04750-4.
92. Zhao, D.; Cai, C. Layered Ti_3C_2 MXene Modified Two-Dimensional Bi_2WO_6 Composites with Enhanced Visible Light Photocatalytic Performance. *Mater. Chem. Front.* **2019**, *3*, 2521–2528, doi:10.1039/C9QM00570F.
93. Akbari, M.; Rasouli, J.; Rasouli, K.; Ghaedi, S.; Mohammadi, M.; Rajabi, H.; Sabbaghi, S. MXene-Based Composite Photocatalysts for Efficient Degradation of Antibiotics in Wastewater. *Sci. Rep.* **2024**, *14*, 31498, doi:10.1038/s41598-024-83333-3.
94. Yao, J.; Wang, C. Decolorization of Methylene Blue with TiO 2 Sol via UV Irradiation Photocatalytic Degradation. *Int. J. Photoenergy* **2010**, *2010*, 1–6, doi:10.1155/2010/643182.
95. Othman, Z.; Sinopoli, A.; Mackey, H.R.; Mahmoud, K.A. Efficient Photocatalytic Degradation of Organic Dyes by $AgNPs/TiO_2/Ti_3C_2T_x$ MXene Composites under UV and Solar Light. *ACS Omega* **2021**, *6*, 33325–33338, doi:10.1021/acsomega.1c03189.
96. Kalaiselvi, C.; Krishna Chandar, N. Accordion-like Multilayer $Ti_3C_2T_x$ MXene Sheets Decorated 1D Mn_2O_3 Nanorods-Based Nanocomposites: An Efficient Catalyst for Swift Removal of Single and Mixed Dyes. *J. Phys. Chem. Solids* **2023**, *182*, 111591, doi:10.1016/j.jpcs.2023.111591.
97. Chandiran, K.; Pandian, M.S.; Balakrishnan, S.; Pitchaimuthu, S.; Chen, Y.-S.; Nagamuthu Raja, K.C. $Ti_3C_2T_x$ MXene Decorated with NiMnO3 / NiMn2O4 Nanoparticles for Simultaneous Photocatalytic Degradation

 doi:10.20944/preprints202502.1240.v1

of Mixed Cationic and Anionic Dyes. *Colloids Surf. Physicochem. Eng. Asp.* **2024**, *692*, 133888, doi:10.1016/j.colsurfa.2024.133888.

98. Wang, Y.; Chen, J.; Que, M.; Wu, Q.; Wang, X.; Zhou, Y.; Ma, Y.; Li, Y.; Yang, X. MXene-Derived $Ti_3C_2T_x$ /Bi4Ti3O12 Heterojunction Photocatalyst for Enhanced Degradation of Tetracycline Hydrochloride, Rhodamine B, and Methyl Orange under Visible-Light Irradiation. *Appl. Surf. Sci.* **2023**, *639*, 158270, doi:10.1016/j.apsusc.2023.158270.
99. Lu, Y.; Yao, M.; Zhou, A.; Hu, Q.; Wang, L. Preparation and Photocatalytic Performance of Ti_3C_2 /TiO_2 /CuO Ternary Nanocomposites. *J. Nanomater.* **2017**, *2017*, 1–5, doi:10.1155/2017/1978764.
100. Chen, L.; Ye, X.; Chen, S.; Ma, L.; Wang, Z.; Wang, Q.; Hua, N.; Xiao, X.; Cai, S.; Liu, X. Ti_3C_2 MXene Nanosheet/TiO_2 Composites for Efficient Visible Light Photocatalytic Activity. *Ceram. Int.* **2020**, *46*, 25895–25904, doi:10.1016/j.ceramint.2020.07.074.
101. Nasri, M.S.I.; Samsudin, M.F.R.; Tahir, A.A.; Sufian, S. Effect of MXene Loaded on G-C_3N_4 Photocatalyst for the Photocatalytic Degradation of Methylene Blue. *Energies* **2022**, *15*, 955, doi:10.3390/en15030955.
102. Ayub, A.; Kim, B.; Lim, Y.; Devarayapalli, K.C.; Kim, G.; Lee, D.S. Hydrothermal Synthesis of Cobalt Ferrite-Functionalized $Ti_3C_2T_x$ MXene for the Degradation of Congo Red via Peroxymonosulfate Activation System. *J. Alloys Compd.* **2023**, *963*, 171294, doi:10.1016/j.jallcom.2023.171294.
103. Tariq, A.; Ali, S.I.; Akinwande, D.; Rizwan, S. Efficient Visible-Light Photocatalysis of 2D-MXene Nanohybrids with Gd^{3+} - and Sn^{4+} -Codoped Bismuth Ferrite. *ACS Omega* **2018**, *3*, 13828–13836, doi:10.1021/acsomega.8b01951.
104. Xu, T.; Wang, J.; Cong, Y.; Jiang, S.; Zhang, Q.; Zhu, H.; Li, Y.; Li, X. Ternary BiOBr/TiO_2/Ti_3C_2T MXene Nanocomposites with Heterojunction Structure and Improved Photocatalysis Performance. *Chin. Chem. Lett.* **2020**, *31*, 1022–1025, doi:10.1016/j.cclet.2019.11.038.
105. Liu, X.; Liu, Q.; Chen, C. Ultrasonic Oscillation Synthesized ZnS Nanoparticles/Layered MXene Sheet with Outstanding Photocatalytic Activity under Visible Light. *Vacuum* **2021**, *183*, 109834, doi:10.1016/j.vacuum.2020.109834.
106. Chen, L.; Ye, X.; Chen, S.; Ma, L.; Wang, Z.; Wang, Q.; Hua, N.; Xiao, X.; Cai, S.; Liu, X. Ti_3C_2 MXene Nanosheet/TiO_2 Composites for Efficient Visible Light Photocatalytic Activity. *Ceram. Int.* **2020**, *46*, 25895–25904, doi:10.1016/j.ceramint.2020.07.074.
107. Lemos, H.G.; Ronchi, R.M.; Portugal, G.R.; Rossato, J.H.H.; Selopal, G.S.; Barba, D.; Venancio, E.C.; Rosei, F.; Arantes, J.T.; F. Santos, S. Efficient $Ti_3C_2T_x$ MXene/TiO_2 Hybrid Photoanodes for Dye-Sensitized Solar Cells. *ACS Appl. Energy Mater.* **2022**, *5*, 15928–15938, doi:10.1021/acsaem.2c03474.
108. Yang, J.; Zhu, Q.; Xie, Z.; Wang, Y.; Wang, J.; Peng, Y.; Fang, Y.; Deng, L.; Xie, T.; Xu, L. Enhancement Mechanism of Photocatalytic Activity for MoS2/Ti_3C_2 Schottky Junction: Experiment and DFT Calculation. *J. Alloys Compd.* **2021**, *887*, 161411, doi:10.1016/j.jallcom.2021.161411.
109. Liu, D.; Li, C.; Ge, J.; Zhao, C.; Zhao, Q.; Zhang, F.; Ni, T.; Wu, W. 3D Interconnected G-C_3N_4 Hybridized with 2D Ti_3C_2 MXene Nanosheets for Enhancing Visible Light Photocatalytic Hydrogen Evolution and Dye Contaminant Elimination. *Appl. Surf. Sci.* **2022**, *579*, 152180, doi:10.1016/j.apsusc.2021.152180.
110. Cheng, X.; Liao, J.; Xue, Y.; Lin, Q.; Yang, Z.; Yan, G.; Zeng, G.; Sengupta, A. Ultrahigh-Flux and Self-Cleaning Composite Membrane Based on BiOCl-PPy Modified MXene Nanosheets for Contaminants Removal from Wastewater. *J. Membr. Sci.* **2022**, *644*, 120188, doi:10.1016/j.memsci.2021.120188.
111. Wang, B.; Lin, L.; Chen, Y.; Yang, Q.; Xiong, Y.; Zhang, L.; Dai, X.; Jiang, Y.; Zhong, C.; Liao, J.; et al. Rational Construction of S-Scheme Pt-MnO_2/TiO_2@$Ti_3C_2T_x$ via Ti-O-Mn Bond for Distinguished Charge Transfer in Photocatalytic Wastewater Environmental Governance and Hydrogen Production. *Compos. Sci. Technol.* **2023**, *241*, 110137, doi:10.1016/j.compscitech.2023.110137.
112. Lin, Q.; Zeng, G.; Yan, G.; Luo, J.; Cheng, X.; Zhao, Z.; Li, H. Self-Cleaning Photocatalytic MXene Composite Membrane for Synergistically Enhanced Water Treatment: Oil/Water Separation and Dyes Removal. *Chem. Eng. J.* **2022**, *427*, 131668, doi:10.1016/j.cej.2021.131668.
113. Khadidja, M.F.; Fan, J.; Li, S.; Li, S.; Cui, K.; Wu, J.; Zeng, W.; Wei, H.; Jin, H.-G.; Naik, N.; et al. Hierarchical ZnO/MXene Composites and Their Photocatalytic Performances. *Colloids Surf. Physicochem. Eng. Asp.* **2021**, *628*, 127230, doi:10.1016/j.colsurfa.2021.127230.

 doi:10.20944/preprints202502.1240.v1

114. Xue, H.; Yan, Q.; Chen, L.; Wang, Y.; Xie, X.; Sun, J. Ti_3C_2 MXene Assembled with TiO_2 for Efficient Photocatalytic Mineralization of Gaseous O-Xylene. *Appl. Surf. Sci.* **2023**, *608*, 155136, doi:10.1016/j.apsusc.2022.155136.
115. Hieu, V.Q.; Phung, T.K.; Nguyen, T.-Q.; Khan, A.; Doan, V.D.; Tran, V.A.; Le, V.T. Photocatalytic Degradation of Methyl Orange Dye by Ti_3C_2–TiO_2 Heterojunction under Solar Light. *Chemosphere* **2021**, *276*, 130154, doi:10.1016/j.chemosphere.2021.130154.
116. Mousavi, S.M.; Mohtaram, M.S.; Rasouli, K.; Mohtaram, S.; Rajabi, H.; Sabbaghi, S. Efficient Visible-Light-Driven Photocatalytic Degradation of Antibiotics in Water by MXene-Derived TiO_2-Supported SiO_2 /Ti_3C_2 Composites: Optimisation, Mechanism and Toxicity Evaluation. *Environ. Pollut.* **2025**, *367*, 125624, doi:10.1016/j.envpol.2024.125624.
117. Huang, G.; Li, S.; Liu, L.; Zhu, L.; Wang, Q. Ti_3C_2 MXene-Modified Bi2WO6 Nanoplates for Efficient Photodegradation of Volatile Organic Compounds. *Appl. Surf. Sci.* **2020**, *503*, 144183, doi:10.1016/j.apsusc.2019.144183.
118. Zhou, X.; Liu, G.; Yu, J.; Fan, W. Surface Plasmon Resonance-Mediated Photocatalysis by Noble Metal-Based Composites under Visible Light. *J. Mater. Chem.* **2012**, *22*, 21337, doi:10.1039/c2jm31902k.
119. Qin, J.; Hu, X.; Li, X.; Yin, Z.; Liu, B.; Lam, K. 0D/2D $AgInS_2$/MXene Z-Scheme Heterojunction Nanosheets for Improved Ammonia Photosynthesis of N2. *Nano Energy* **2019**, *61*, 27–35, doi:10.1016/j.nanoen.2019.04.028.
120. Yusuf, B.O.; Umar, M.; Aliyu, M.; Alhassan, A.M.; Awad, M.M.; Taialla, O.A.; Abdullahi, A.S.; Musa, J.N.; Alhooshani, K.R.; Ganiyu, S.A. Recent Advances and Future Prospects of MXene-Based Photocatalysts in Environmental Remediations. *J. Environ. Chem. Eng.* **2024**, *12*, 114812, doi:10.1016/j.jece.2024.114812.
121. Hassaan, M.A.; El-Nemr, M.A.; Elkatory, M.R.; Ragab, S.; Niculescu, V.-C.; El Nemr, A. Principles of Photocatalysts and Their Different Applications: A Review. *Top. Curr. Chem.* **2023**, *381*, 31, doi:10.1007/s41061-023-00444-7.
122. Kuang, P.; Low, J.; Cheng, B.; Yu, J.; Fan, J. MXene-Based Photocatalysts. *J. Mater. Sci. Technol.* **2020**, *56*, 18–44, doi:10.1016/j.jmst.2020.02.037.
123. Parwaiz, S.; Sohn, Y.; Khan, M.M. Insights into MXenes and MXene-Based Heterostructures for Various Photocatalytic Applications. *Mater. Sci. Semicond. Process.* **2025**, *186*, 109099, doi:10.1016/j.mssp.2024.109099.
124. You, Z.; Liao, Y.; Li, X.; Fan, J.; Xiang, Q. State-of-the-Art Recent Progress in MXene-Based Photocatalysts: A Comprehensive Review. *Nanoscale* **2021**, *13*, 9463–9504, doi:10.1039/D1NR02224E.
125. Kumar, A.; Majithia, P.; Choudhary, P.; Mabbett, I.; Kuehnel, M.F.; Pitchaimuthu, S.; Krishnan, V. MXene Coupled Graphitic Carbon Nitride Nanosheets Based Plasmonic Photocatalysts for Removal of Pharmaceutical Pollutant. *Chemosphere* **2022**, *308*, 136297, doi:10.1016/j.chemosphere.2022.136297.
126. Diao, Y.; Yan, M.; Li, X.; Zhou, C.; Peng, B.; Chen, H.; Zhang, H. In-Situ Grown of g-C_3N_4 /Ti_3C_2/TiO_2 Nanotube Arrays on Ti Meshes for Efficient Degradation of Organic Pollutants under Visible Light Irradiation. *Colloids Surf. Physicochem. Eng. Asp.* **2020**, *594*, 124511, doi:10.1016/j.colsurfa.2020.124511.
127. Zhou, Y.; Yu, M.; Zhan, R.; Wang, X.; Peng, G.; Niu, J. Ti_3C_2 MXene-Induced Interface Electron Separation in g-C_3N_4/Ti_3C_2 MXene/MoSe2 Z-Scheme Heterojunction for Enhancing Visible Light-Irradiated Enoxacin Degradation. *Sep. Purif. Technol.* **2021**, *275*, 119194, doi:10.1016/j.seppur.2021.119194.
128. Rdewi, E.H.; Abbas, K.K.; AbdulkadhimAl-Ghaban, A.M.H. Removal Pharmaceutical Carbamazepine from Wastewater Using ZnO-TiO_2-MXene Heterostructural Nanophotocatalyst under Solar Light Irradiation. *Mater. Today Proc.* **2022**, *60*, 1702–1711, doi:10.1016/j.matpr.2021.12.229.
129. Abbas, K.K.; AbdulkadhimAl-Ghaban, A.M.H.; Rdewi, E.H. Synthesis of a Novel ZnO/TiO_2-Nanorod MXene Heterostructured Nanophotocatalyst for the Removal Pharmaceutical Ceftriaxone Sodium from Aqueous Solution under Simulated Sunlight. *J. Environ. Chem. Eng.* **2022**, *10*, 108111, doi:10.1016/j.jece.2022.108111.
130. Sukidpaneenid, S.; Chawengkijwanich, C.; Pokhum, C.; Isobe, T.; Opaprakasit, P.; Sreearunothai, P. Multi-Function Adsorbent-Photocatalyst MXene-TiO_2 Composites for Removal of Enrofloxacin Antibiotic from Water. *J. Environ. Sci.* **2023**, *124*, 414–428, doi:10.1016/j.jes.2021.09.042.

131. Shahzad, A.; Rasool, K.; Nawaz, M.; Miran, W.; Jang, J.; Moztahida, M.; Mahmoud, K.A.; Lee, D.S. Heterostructural $TiO_2/Ti_3C_2T_x$ (MXene) for Photocatalytic Degradation of Antiepileptic Drug Carbamazepine. *Chem. Eng. J.* **2018**, *349*, 748–755, doi:10.1016/j.cej.2018.05.148.
132. Mohanty, S.; Sharma, M.; Kumar, A.; Krishnan, V. Hot Electron-Mediated Photocatalytic Degradation of Ciprofloxacin Using Au-Decorated $SrTiO_3$ - and Ti_3C_2 MXene-Based Interfacial Heterostructure Nanoarchitectonics. *J. Phys. Chem. C* **2023**, *127*, 17711–17722, doi:10.1021/acs.jpcc.3c03573.
133. Du, X.; Ye, L.; Zhu, J.; Ye, Y.; Wang, A.; Zhang, H.; Xu, Z.; Dai, L.; Wang, Y. Novel Cerium (IV) Oxide - Ti_3C_2- Titanium Dioxide Heterostructure Photocatalyst for Pharmaceutical Pollutants Removal: Photocatalyst Characterization, Process Optimization and Transformation Pathways. *Surf. Interfaces* **2024**, *46*, 103892, doi:10.1016/j.surfin.2024.103892.
134. Sergiienko, S.A.; Tobaldi, D.M.; Lajaunie, L.; Lopes, D.V.; Constantinescu, G.; Shaula, A.L.; Shcherban, N.D.; Shkepu, V.I.; Calvino, J.J.; Frade, J.R.; et al. Correction: Photocatalytic Removal of Benzene over $Ti_3C_2T_x$ MXene and TiO_2 –MXene Composite Materials under Solar and NIR Irradiation. *J. Mater. Chem. C* **2023**, *11*, 5225–5225, doi:10.1039/D3TC90070C.
135. Mo, H.; Wang, Y. A Bionic Solar-Driven Interfacial Evaporation System with a Photothermal-Photocatalytic Hydrogel for VOC Removal during Solar Distillation. *Water Res.* **2022**, *226*, 119276, doi:10.1016/j.watres.2022.119276.
136. Mishra, R.P.; Mrinalini, M.; Kumar, N.; Bastia, S.; Chaudhary, Y.S. Efficient Photocatalytic CO_2 Reduction with High Selectivity for Ethanol by Synergistically Coupled MXene-Ceria and the Charge Carrier Dynamics. *Langmuir* **2023**, *39*, 14189–14203, doi:10.1021/acs.langmuir.3c01064.
137. Sun, Y.; Meng, X.; Dall'Agnese, Y.; Dall'Agnese, C.; Duan, S.; Gao, Y.; Chen, G.; Wang, X.-F. 2D MXenes as Co-Catalysts in Photocatalysis: Synthetic Methods. *Nano-Micro Lett.* **2019**, *11*, 79, doi:10.1007/s40820-019-0309-6.
138. Cao, S.; Shen, B.; Tong, T.; Fu, J.; Yu, J. 2D/2D Heterojunction of Ultrathin MXene/Bi_2WO_6 Nanosheets for Improved Photocatalytic CO_2 Reduction. *Adv. Funct. Mater.* **2018**, *28*, 1800136, doi:10.1002/adfm.201800136.
139. Li, J.; Wang, Y.; Wang, Y.; Guo, Y.; Zhang, S.; Song, H.; Li, X.; Gao, Q.; Shang, W.; Hu, S.; et al. MXene Ti_3C_2 Decorated G-C_3N_4/ZnO Photocatalysts with Improved Photocatalytic Performance for CO_2 Reduction. *Nano Mater. Sci.* **2023**, *5*, 237–245, doi:10.1016/j.nanoms.2023.02.003.
140. Irfan, M.; Ahmad, I.; Shukrullah, S.; Hussain, H.; Atif, M.; Legutko, S.; Petru, J.; Hatala, M.; Naz, M.Y.; Rahman, S. Construction of 0D/2D Schottky Heterojunctions of ZnO and Ti_3C_2 Nanosheets with the Enriched Transfer of Interfacial Charges for Photocatalytic Hydrogen Evolution. *Materials* **2022**, *15*, 4557, doi:10.3390/ma15134557.
141. Colmenares, J.; Kuna, E. Photoactive Hybrid Catalysts Based on Natural and Synthetic Polymers: A Comparative Overview. *Molecules* **2017**, *22*, 790, doi:10.3390/molecules22050790.
142. Peng, Y.; Cai, P.; Yang, L.; Liu, Y.; Zhu, L.; Zhang, Q.; Liu, J.; Huang, Z.; Yang, Y. Theoretical and Experimental Studies of Ti_3C_2 MXene for Surface-Enhanced Raman Spectroscopy-Based Sensing. *ACS Omega* **2020**, *5*, 26486–26496, doi:10.1021/acsomega.0c03009.
143. Hosseini, S.F.; Seyed Dorraji, M.S.; Rasoulifard, M.H. Boosting Photo-Charge Transfer in 3D/2D TiO_2@Ti_3C_2 MXene/Bi2S3 Schottky/Z-Scheme Heterojunction for Photocatalytic Antibiotic Degradation and H2 Evolution. *Compos. Part B Eng.* **2023**, *262*, 110820, doi:10.1016/j.compositesb.2023.110820.
144. Hieu, V.Q.; Phung, T.K.; Nguyen, T.-Q.; Khan, A.; Doan, V.D.; Tran, V.A.; Le, V.T. Photocatalytic Degradation of Methyl Orange Dye by Ti_3C_2–TiO_2 Heterojunction under Solar Light. *Chemosphere* **2021**, *276*, 130154, doi:10.1016/j.chemosphere.2021.130154.
145. Wang, D.; Zhao, L.; Song, D.; Qiu, J.; Kong, F.; Guo, L.-H. A Formation Model of Superoxide Radicals Photogenerated in Nano-TiO_2 Suspensions. *RSC Adv.* **2019**, *9*, 29429–29432, doi:10.1039/C9RA06323D.
146. Zhang, S.; Cai, M.; Wu, J.; Wang, Z.; Lu, X.; Li, K.; Lee, J.-M.; Min, Y. Photocatalytic Degradation of TiO_2 via Incorporating Ti_3C_2 MXene for Methylene Blue Removal from Water. *Catal. Commun.* **2023**, *174*, 106594, doi:10.1016/j.catcom.2022.106594.

147. Farghaly, A.; Maher, E.; Gad, A.; El-Bery, H. Synergistic Photocatalytic Degradation of Methylene Blue Using TiO_2 Composites with Activated Carbon and Reduced Graphene Oxide: A Kinetic and Mechanistic Study. *Appl. Water Sci.* **2024**, *14*, 228, doi:10.1007/s13201-024-02286-0.
148. Islam Molla, Md.A.; Tateishi, I.; Furukawa, M.; Katsumata, H.; Suzuki, T.; Kaneco, S. Evaluation of Reaction Mechanism for Photocatalytic Degradation of Dye with Self-Sensitized TiO₂ under Visible Light Irradiation. *Open J. Inorg. Non-Met. Mater.* **2017**, *07*, 1–7, doi:10.4236/ojinm.2017.71001.
149. Kumar Mandal, R.; Ghosh, S.; Pal Majumder, T. Comparative Study between Degradation of Dyes (MB, MO) in Monotonous and Binary Solution Employing Synthesized Bimetallic (Fe-CdO) NPs Having Antioxidant Property. *Results Chem.* **2023**, *5*, 100788, doi:10.1016/j.rechem.2023.100788.
150. Cao, F.; Zhang, Y.; Wang, H.; Khan, K.; Tareen, A.K.; Qian, W.; Zhang, H.; Ågren, H. Recent Advances in Oxidation Stable Chemistry of 2D MXenes. *Adv. Mater.* **2022**, *34*, 2107554, doi:10.1002/adma.202107554.